



HAL
open science

Isotopic composition of CO₂ in the atmosphere of Mars: fractionation by diffusive separation observed by the ExoMars Trace Gas Orbiter

Juan Alday, Colin F. Wilson, Patrick G. J. Irwin, Alexander Trokhimovskiy,
Franck Montmessin, Anna A. Fedorova, Denis A. Belyaev, Kevin S. Olsen,
Oleg Korablev, Franck Lefèvre, et al.

► To cite this version:

Juan Alday, Colin F. Wilson, Patrick G. J. Irwin, Alexander Trokhimovskiy, Franck Montmessin, et al.. Isotopic composition of CO₂ in the atmosphere of Mars: fractionation by diffusive separation observed by the ExoMars Trace Gas Orbiter. *Journal of Geophysical Research. Planets*, 2021, 127 (12), pp.e2021JE006992. 10.1029/2021je006992 . insu-03473299v1

HAL Id: insu-03473299

<https://insu.hal.science/insu-03473299v1>

Submitted on 9 Dec 2021 (v1), last revised 19 Dec 2021 (v2)

HAL is a multi-disciplinary open access archive for the deposit and dissemination of scientific research documents, whether they are published or not. The documents may come from teaching and research institutions in France or abroad, or from public or private research centers.

L'archive ouverte pluridisciplinaire **HAL**, est destinée au dépôt et à la diffusion de documents scientifiques de niveau recherche, publiés ou non, émanant des établissements d'enseignement et de recherche français ou étrangers, des laboratoires publics ou privés.



Distributed under a Creative Commons Attribution 4.0 International License

1 **Isotopic composition of CO₂ in the atmosphere of**
2 **Mars: fractionation by diffusive separation observed by**
3 **the ExoMars Trace Gas Orbiter**

4 **Juan Alday¹, Colin F. Wilson¹, Patrick G. J. Irwin¹, Alexander**
5 **Trokhimovskiy², Franck Montmessin³, Anna A. Fedorova², Denis A. Belyaev²,**
6 **Kevin S. Olsen¹, O. Korablev², Franck Lefvre³, Ashwin S. Braude³, Lucio**
7 **Baggio³, Andrey Patrakeev² and Alexey Shakun²**

8 ¹AOPP, Department of Physics, University of Oxford, Oxford, United Kingdom

9 ²Space Research Institute (IKI), Moscow, Russia

10 ³LATMOS/CNRS, Guyancourt, France

11 **Key Points:**

- 12 • Isotopic ratios in CO₂ are observed to be consistent with telluric standards and
13 to fractionate by diffusive separation above the homopause.
14 • At least 20-40% of the C reservoir has escaped to space throughout Martian his-
15 tory.
16 • The higher ¹⁸O/¹⁶O ratio in H₂O than in CO₂ may be explained by a photochem-
17 ical transfer of lighter O from H₂O to CO₂.

Corresponding author: Juan Alday, juan.aldayparejo@physics.ox.ac.uk

This article has been accepted for publication and undergone full peer review but has not been through the copyediting, typesetting, pagination and proofreading process, which may lead to differences between this version and the [Version of Record](#). Please cite this article as [doi: 10.1029/2021JE006992](https://doi.org/10.1029/2021JE006992).

This article is protected by copyright. All rights reserved.

Abstract

Isotopic ratios in atmospheric CO₂ are shaped by various processes throughout Mars' history, and can help understand what the atmosphere of early Mars was like to sustain liquid water on its surface. In this study, we monitor the O and C isotopic composition of CO₂ between 70 and 130 km for more than half a Martian year using solar occultation observations by the Atmospheric Chemistry Suite onboard the ExoMars Trace Gas Orbiter. We find the vertical trends of the isotopic ratios to be consistent with the expectations from diffusive separation above the homopause, with average values below this altitude being consistent with Earth-like fractionation ($\delta^{13}\text{C} = -3 \pm 37 \text{‰}$; $\delta^{18}\text{O} = -29 \pm 38 \text{‰}$; $\delta^{17}\text{O} = -11 \pm 41 \text{‰}$). Using these measurements, we estimate that at least 20-40% of primordial C on Mars has escaped to space throughout history. The total amount of C lost from the atmosphere is likely to be well in excess of this lower limit, due to carbonate formation and further sink processes. In addition, we propose a photochemical transfer of light O from H₂O to CO₂ to explain the larger enrichment in the ¹⁸O/¹⁶O ratio in H₂O than in CO₂.

Plain Language Summary

There is ample evidence suggesting that liquid water was abundant on the surface of Mars in the past. However, climatic conditions on early Mars must have been very different from the ones we observe today in order to sustain liquid water on its surface. The ratios of the heavy and light isotopes in different species provide a very useful tool to estimate the early climate of Mars. In this study, we monitor the isotopic ratios of carbon dioxide in the atmosphere of Mars to provide more accurate estimates of these. With our measurements, and in context with previous studies, we estimate that at least 20-40% of the carbon reservoir has been lost to space throughout Martian history. This, together with the sequestration of atmospheric C on the surface in the form of minerals, is consistent with the idea that the atmosphere of early Mars was denser than the one we observe today.

1 Introduction

Numerous pieces of mineralogical and geomorphological evidence suggest that liquid water was once abundant on the surface of Mars (e.g., Carr & Clow, 1981; Baker, 2001). The presence of large amounts of liquid water on the surface require climatic conditions very different from those resulting from the dry and thin atmosphere Mars has today. In fact, it is still not well understood how the past Martian atmosphere was able to produce sufficient greenhouse warming to sustain liquid water on the surface, nor what drove the transition of the climate to the one we observe today. Although the composition of this early atmosphere remains unknown, carbon dioxide is thought to have been an important contributor to the total atmospheric pressure required to sustain liquid water on the surface, which later on migrated to non-atmospheric reservoirs in the surface or subsurface, or was lost to space (Wordsworth et al., 2013; Ramirez et al., 2014). Enrichment in the heavy isotopes of atmospheric species such as hydrogen, nitrogen or the noble gases with respect to Earth suggest that this transition was driven by the escape of a large portion of the atmosphere to space (e.g., Owen et al., 1977; Jakosky, 1997; Mahaffy et al., 2013). Isotope ratios can provide valuable constraints on the amount of atmosphere that existed in the past, but require a very detailed knowledge of the present-day isotopic ratios and the relative rates by which the different isotopologues of each species escape to space.

The isotopic composition of CO₂ in the atmosphere of Mars has been measured in several instances using both remote sensing and *in situ* techniques. Isotopic ratios are usually given as a deviation of the measured ratio R with respect to a standard R_s in units of per mil (e.g., $\delta^{13}\text{C} = (R/R_s - 1) \times 1000$). The standard ratios representative

of telluric values are defined by the Vienna Standard Mean Ocean Water (VSMOW) for oxygen ($^{18}\text{O}/^{16}\text{O} = 2005.2 \times 10^{-6}$, $^{17}\text{O}/^{16}\text{O} = 379.9 \times 10^{-6}$), and the Vienna Pee Dee Belemnite (VPDB) for carbon ($^{13}\text{C}/^{12}\text{C} = 1.123 \times 10^{-2}$). Measurements made using the neutral mass spectrometers on the Viking aeroshell and landers revealed the oxygen and carbon isotope composition of Mars' atmosphere to be consistent with Earth within 5% (i.e., $\delta^{13}\text{C} = \delta^{18}\text{O} = 0 \pm 50\%$) (Nier & McElroy, 1977; Owen, 1982). Early ground-based high resolution spectroscopic measurements revealed a possible depletion of the ratios in CO_2 with respect to Earth ($\delta^{13}\text{C} = -73 \pm 58\%$; $\delta^{18}\text{O} = -40 \pm 130\%$, Schrey et al. (1986); $\delta^{13}\text{C} = -73 \pm 58\%$; $\delta^{18}\text{O} = -130 \pm 80\%$, Krasnopolsky et al. (1996)), but more recent observations showed only marginal deviations with respect to the standard ($\delta^{13}\text{C} = 0 \pm 110\%$, Encrenaz et al. (2005); $\delta^{13}\text{C} = -22 \pm 20\%$; $\delta^{18}\text{O} = 18 \pm 18\%$, Krasnopolsky et al. (2007)). The most precise measurements of the C and O isotope composition in the Martian atmosphere were made by the Phoenix Lander and the Curiosity Rover, but observing two different values whose uncertainty ranges did not overlap. Niles et al. (2010) found carbon dioxide to be enriched in ^{18}O but not ^{13}C ($\delta^{13}\text{C} = -2.5 \pm 4.3\%$; $\delta^{18}\text{O} = 31.0 \pm 5.7\%$) using measurements with the Thermal Evolved Gas Analyzer (TEGA) mass spectrometer on the Phoenix Lander. However, reconsideration of these data suggest that the lack of measured enrichment in ^{13}C may be a measurement artifact (Niles et al., 2014). On the other hand, Webster et al. (2013) reported similar enrichments in $\delta^{13}\text{C}$ and $\delta^{18}\text{O}$ ($\delta^{13}\text{C} = 46 \pm 4\%$; $\delta^{18}\text{O} = 48 \pm 5\%$) using measurements made with the Sample Analysis at Mars' Tunable Laser Spectrometer (SAM/TLS) on the Curiosity Rover. The observed enrichment in $\delta^{13}\text{C}$ was confirmed by Mahaffy et al. (2013) using SAM's quadrupole mass spectrometer (SAM/QMS) ($\delta^{13}\text{C} = 45 \pm 12\%$).

The only evidence of variability in the isotope ratios of CO_2 was recently reported by Livengood et al. (2020) using ground-based spectroscopic observations, which revealed variations from $\delta^{18}\text{O} = -92 \pm 23\%$ to $\delta^{18}\text{O} = 71 \pm 18\%$ over a temperature increase from 266.9 K to 275.4 K. The observed correlation between the oxygen isotopic ratios and the surface temperature could be indicative of fractionation during the adsorption of CO_2 on the Martian regolith (Rahn & Eiler, 2001; Livengood et al., 2020). The average isotopic ratio was reported to be consistent with Earth-like fractionation within the measured uncertainties ($\delta^{18}\text{O} = 9 \pm 14\%$), which stresses the need of understanding the variations of the isotopic ratios to disentangle the ratios representative of the whole atmospheric reservoir from those derived in localised measurements.

Because CO_2 is the major reservoir of C in the Martian atmosphere, the $^{13}\text{C}/^{12}\text{C}$ isotopic ratio in CO_2 can be used to estimate the escape of C through time. Hu et al. (2015) modelled the isotopic fractionation induced by atmospheric loss, outgassing and carbonate formation through time, analysing the likelihood of different combinations of these to match the observed isotopic ratio in CO_2 at present, which is assumed to be the value reported from the measurements by the Curiosity Rover. This methodology suggests the presence of an early atmosphere with a surface pressure < 1 bar, with denser atmospheric scenarios requiring large amounts of carbonate formation. Jakosky (2019) also estimated the fraction of the C reservoir lost to space throughout history, suggesting that this process could have removed 1-2 bars of CO_2 . While these estimates are higher than those reported by Hu et al. (2015), Jakosky (2019) notes that this discrepancy can be explained by extrapolating the results to the same epoch (~ 4.3 billion years ago), where the results of Hu et al. (2015) would also indicate a loss of 1.0-1.7 bars of CO_2 .

In this study, we monitor the C and O isotopic ratios in CO_2 in an altitude range of 70-130 km for more than half a Martian year (MY) using solar occultation observations made by the Atmospheric Chemistry Suite (ACS) onboard the ExoMars Trace Gas Orbiter (TGO). These measurements allow the determination of vertical profiles for each of the isotopic ratios, enabling the determination of altitude-dependant fractionation processes, and the estimation of the isotopic composition of CO_2 representative of the atmospheric reservoir outside of fractionation processes. In addition, we discuss the im-

121 plications of our measurements to the evolution of CO₂ in the Martian atmosphere, as
 122 well as the implications of the different O isotopic ratios in H₂O and CO₂.

123 2 ACS Solar Occultation Measurements

124 The Atmospheric Chemistry Suite combines three infrared spectrometers covering
 125 a total spectral range of 0.7-17 μm (Korablev et al., 2018). The mid-infrared channel (MIR),
 126 used in this study, is an echelle cross-dispersion spectrometer dedicated to solar occul-
 127 tation measurements between 2.3 and 4.2 μm (2380-4350 cm^{-1}). In order to achieve high
 128 spectral resolution ($\lambda/\Delta\lambda \sim 30000$) measurements in a broad instantaneous spectral range
 129 (0.15-0.3 μm) within the whole spectral range of the instrument, ACS MIR incorporates
 130 a movable secondary grating that allows the selection of diffraction orders. These diffrac-
 131 tion orders are then projected along the vertical coordinate of a 640×512 pixel detec-
 132 tor frame, while the horizontal coordinate contains the spectral information of the mea-
 133 surement. The width of the diffraction orders along the vertical coordinate expands ~ 20
 134 pixels and represents the illuminated part of the slit (1×9 arcmin). Since the slit is ori-
 135 ented perpendicularly to the surface, the width of each diffraction order represents the
 136 instantaneous field-of-view of the instrument ($\Delta z \sim 4$ km at the tangent point), with
 137 a vertical resolution of approximately 150 m per pixel (see Figure 1a).

138 ACS MIR makes its measurements in the so-called solar occultation mode in which
 139 the Sun is continuously observed by the instrument from an altitude of 270 km until it
 140 is concealed by the Martian surface. The detector frames are recorded every 2.1 s, which
 141 allows the reconstruction of atmospheric vertical profiles with a resolution of 1-3 km, al-
 142 though a finer vertical sampling can be achieved by also making use of the instantaneous
 143 field-of-view of the instrument in each acquisition. The reference solar spectrum, used
 144 to derive the transmission spectra at each altitude, is calculated from the acquisitions
 145 above 190 km. On the other hand, the observations where the solar disk is concealed by
 146 the Martian surface are used to estimate the dark signal (see Figure 1b). Calibration of
 147 the spectra includes an orthorectification of the detector image, the removal of hot pix-
 148 els, the dark signal and the straylight, and a correction for the sub-pixel drift occurring
 149 due to the slightly varying thermal state of the instrument. The spectral calibration of
 150 the measurements is performed by comparing the solar lines with the ACE-FTS solar
 151 atlas (Hase et al., 2010), and then further refined using atmospheric absorption lines of
 152 CO₂.

153 The instrument line shape (ILS) is impacted by an optical aberration in one of the
 154 lenses, causing a doubling of the detector image and consequently of the absorption lines.
 155 The impact of the doubling varies as a function of wavenumber and with detector row.
 156 This effect can be perceived from the spectra shown in Figure 1c: while the transmis-
 157 sion spectrum taken from the slit end (blue line) shows single-peaked absorption lines,
 158 the spectrum from the centre of the stripe (green line) is more affected by the doubling.
 159 The varying nature of the doubling effect requires it to be accounted for in the modelling
 160 of the observations. In this study, the ILS is parameterised using a double Gaussian func-
 161 tion as described by Alday et al. (2019), in which the tuning parameters are fitted in par-
 162 allel with the rest of the atmospheric properties. This approach has been validated against
 163 simultaneous solar occultation measurements of H₂O, CO and CO₂ made by ACS NIR
 164 (Alday et al., 2019; Fedorova et al., 2020; Alday et al., 2021; Olsen et al., 2021).

165 The dataset assembled for the analysis of the isotopic composition of CO₂ in this
 166 study comprises the observations made by ACS MIR using secondary grating position
 167 4 from the start of the science operations in March 2018 to February 2021. This observ-
 168 ing scheme enables the selection of ten diffraction orders (215-224) in a spectral range
 169 between 2.65 and 2.78 μm (36003770 cm^{-1}), which encompass absorption bands of sev-
 170 eral isotopologues of CO₂ and of H₂O. In particular, the spectral region of interest for
 171 the measurement of the isotopic ratios in CO₂ lies in diffraction orders 217-219. Dur-

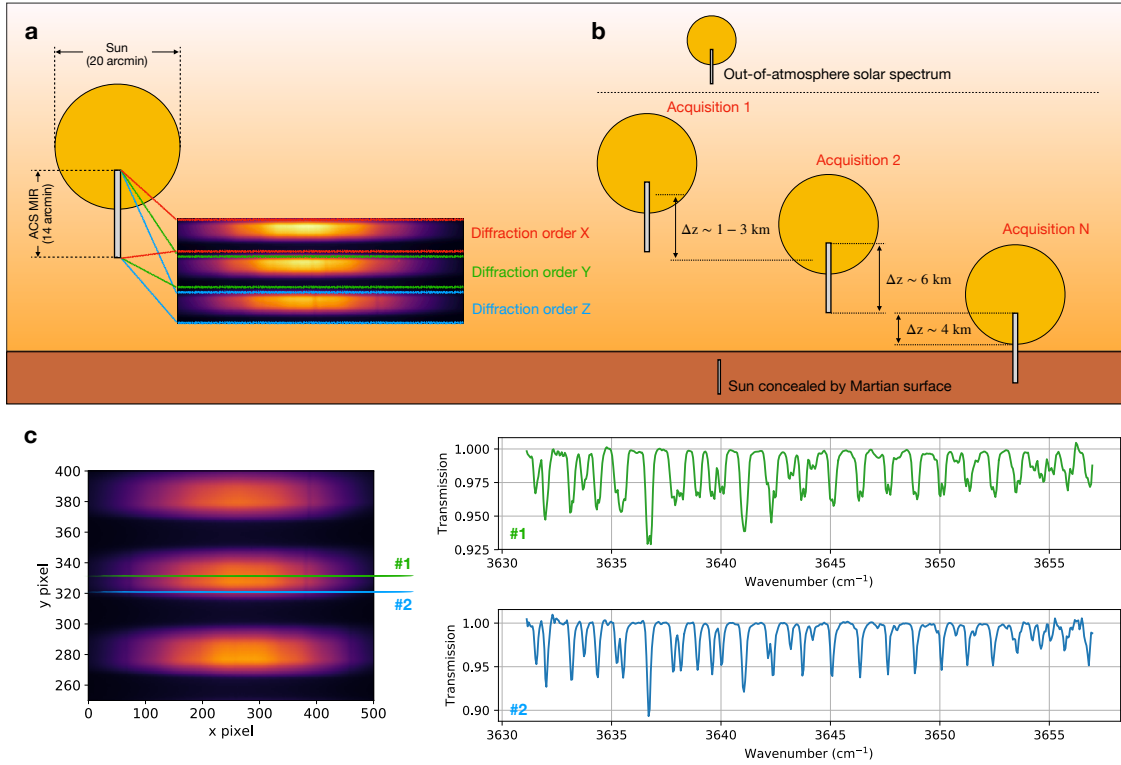


Figure 1. Illustration of the ACS MIR solar occultation observations. a) In each acquisition, a number of diffraction orders are projected onto the detector frame. Since the slit is oriented perpendicularly to the surface of Mars, the width of each of the diffraction orders represents the instantaneous field-of-view of the instrument, with a vertical resolution of ~ 150 m/pixel. b) During a solar occultation, several measurements are made at different tangent heights with a vertical resolution of ~ 1 -3 km, although a finer vertical sampling can be achieved when making use of the instantaneous field-of-view in each of the acquisitions. c) Selection of different rows within the detector frame from one acquisition allow the selection of different spectral ranges, if selecting rows from different diffraction orders, or different tangent altitudes, if selecting different rows from the same diffraction order. The green and blue lines highlight the difference in the instrument lineshape between the rows corresponding to maximum intensity (green) and the slit end (blue) for diffraction order 217.

172 ing a substantial part of the science operations, ACS MIR observations made with sec-
 173 ondary grating position 4 applied the so-called partial framing, in which just a portion
 174 of the detector frame was recorded and sent back to Earth. In these observations, diffrac-
 175 tion orders 217-219 were not recorded, and impede the derivation of the isotopic ratios
 176 in CO₂. Therefore, the dataset assembled for this study comprises the analysis of 246
 177 full-frame observations, which are divided in two periods, one covering the range $L_S =$
 178 $164\text{--}219^\circ$ in Martian year 34 (MY34), and the second one covering the range $L_S = 141\text{--}$
 179 356° in MY35, as shown in Figure 2.

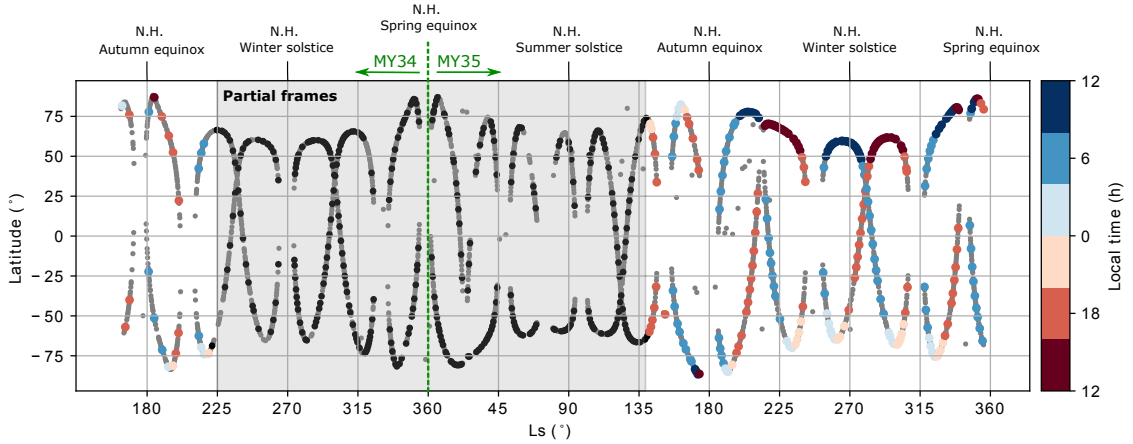


Figure 2. Observational coverage of ACS MIR full frame secondary grating position 4 solar occultation observations. Approximately 14% of all available ACS MIR observations between March 2018 and February 2021 (grey points) were made using secondary grating position 4 (black and coloured points). During part of the science operations, observations were made using partial framing (black points within shaded region), which do not allow the derivation of the CO₂ isotopic ratios. The coloured points, whose colour represents the local time of the observations, are the full-frame observations, which allow the derivation of the CO₂ isotope ratios.

180 3 Radiative Transfer Analysis

181 The radiative transfer analysis of the solar occultation measurements is made us-
 182 ing the NEMESIS (Nonlinear optimal Estimator for MultivariatE spectral analySIS) al-
 183 gorithm (Irwin et al., 2008), which works using the optimal estimation formalism (Rodgers,
 184 2000). In particular, five spectral windows within diffraction orders 217, 218 and 219 (3634.8--
 185 3645.7 cm^{-1} ; $3645.7\text{--}3654\text{ cm}^{-1}$; $3652.5\text{--}3662.5\text{ cm}^{-1}$; $3662.5\text{--}3672\text{ cm}^{-1}$; $3672\text{--}3682\text{ cm}^{-1}$)
 186 are selected to simultaneously retrieve the line-of-sight density of the four major isotopo-
 187 logues of CO₂ ($^{12}\text{C}^{16}\text{O}_2$, $^{13}\text{C}^{16}\text{O}_2$, $^{18}\text{O}^{12}\text{C}^{16}\text{O}$ and $^{17}\text{O}^{12}\text{C}^{16}\text{O}$), which allows the deriva-
 188 tion of the $^{13}\text{C}/^{12}\text{C}$, $^{18}\text{O}/^{16}\text{O}$ and $^{17}\text{O}/^{16}\text{O}$ isotopic ratios. In addition, the parameters
 189 describing the ILS are also simultaneously fitted in each of the five spectral windows sel-
 190 lected for the analysis of the observations.

191 All gaseous absorption in this work is modelled using pre-computed look-up tables
 192 calculated using line-by-line modelling. The spectroscopic parameters of the CO₂ absorp-
 193 tion lines are taken from the 2016 version of the HITRAN database (Gordon et al., 2017),
 194 considering the pressure-broadening coefficients of the different isotopologues are given
 195 solely by self broadening. The partition functions, which determine the statistical prop-
 196 erties of a gas in thermodynamic equilibrium at a given temperature and which are re-
 197 quired to model the intensity of the spectral lines, are taken from Gamache et al. (2017).

198 In the spectral range analysed in this work, the strength of the CO₂ absorption lines is
199 highly sensitive to the atmospheric temperature, which means that this parameter must
200 be known to accurately model the spectra. The atmospheric temperature profile can be
201 retrieved in this spectral range using the CO₂ absorption under the assumptions of a known
202 CO₂ volume mixing ratio and an atmosphere in hydrostatic equilibrium (e.g., Qumerais
203 et al., 2006). Such an approach, previously used for the derivation of the isotopic ratios
204 in H₂O from ACS MIR spectra (Alday et al., 2019, 2021), requires the simultaneous re-
205 trieval of all tangent heights. While this methodology is optimal when using relatively
206 narrow spectral windows, another method can be applied when using a broader spec-
207 tral range. In particular, the rotational temperature of a particular gas can be retrieved
208 by looking at the ratio of different spectral lines within an absorption band, which varies
209 with temperature due to the different dependence to this parameter of the line strengths
210 of each of the transitions (e.g., Mahieux et al., 2010; Olsen et al., 2016). This approach
211 has the advantage of allowing the retrieval of the temperature field at each altitude level
212 independently.

213 We develop a retrieval scheme to simultaneously constrain the rotational temper-
214 ature of CO₂ along with the line-of-sight densities of the different isotopologues from each
215 acquisition made by ACS MIR. In order to perform the retrieval of each acquisition in-
216 dependently and to allow a large number of spectral bands to be fitted simultaneously,
217 we model the gaseous absorption of each transmission spectrum in a single homogeneous
218 path with constant pressure and temperature. However, this assumption limits the verti-
219 cal range under which this approach can be applied. In particular, the assumption of
220 a constant pressure and temperature along the line of sight implies that all absorption
221 occurs at the tangent point, with no contribution from the other atmospheric layers. The
222 averaging kernels provide a measure of the sensitivity of the spectrum along the line of
223 sight. Figure 3 shows the averaging kernels of the vertical profiles of the CO₂ isotopo-
224 logues in our spectral range of interest. These kernels show that the sensitivity of the
225 spectra below 40 km is extended and different for the several isotopologues, which can
226 lead to biases when trying to determine the isotopic ratios. In contrast, the measurements
227 above 60 km show a much narrower spread of the averaging kernels above the tangent
228 height, which is similar for the different isotopologues. In particular, while 75% of the
229 information is confined within 3 km above the tangent height for the measurements above
230 60 km, this number increases to 4 and 10 km for the measurements at 55 and 35 km, re-
231 spectively. Based on these results, we only apply our retrieval scheme to the observations
232 in the upper atmosphere (70-130 km), where the line-of-sight effects are expected to be
233 minimal.

234 In order to evaluate the validity of the simultaneous retrieval of the rotational tem-
235 perature and the line-of-sight densities of the different isotopologues, we perform a se-
236 ries of retrievals on a single spectrum assuming different pressures (10^{-5} - 10^{-9} atm) and
237 temperatures (100-225 K). The results of this test, summarised in Figure 4, show that
238 there is a clear minimum of χ^2 at approximately 140 K, meaning that the rotational tem-
239 perature can be simultaneously retrieved with the rest of the fitting parameters. On the
240 other hand, changing the pressure over several orders of magnitude does not influence
241 the level of agreement between the model and measurement, nor the other retrieved pa-
242 rameters. It is also shown in Figure 4 that the retrieved isotopic ratios are highly sensi-
243 tive to temperature, meaning that a small discrepancy in the temperature field yields
244 a strong bias in the derived ratios, highlighting the importance of the simultaneous re-
245 trieval of the temperature field for an accurate estimation of the isotopic ratios in CO₂.

246 The developed retrieval scheme, including the simultaneous characterisation of the
247 rotational temperature, is applied independently to each acquisition made by ACS MIR
248 above 70 km, which allows the derivation of the atmospheric temperature and the iso-
249 topic ratios at different altitudes above the Martian surface. In order to increase the con-
250 fidence of the retrieved isotopic ratio profiles, we apply the developed scheme to six dif-

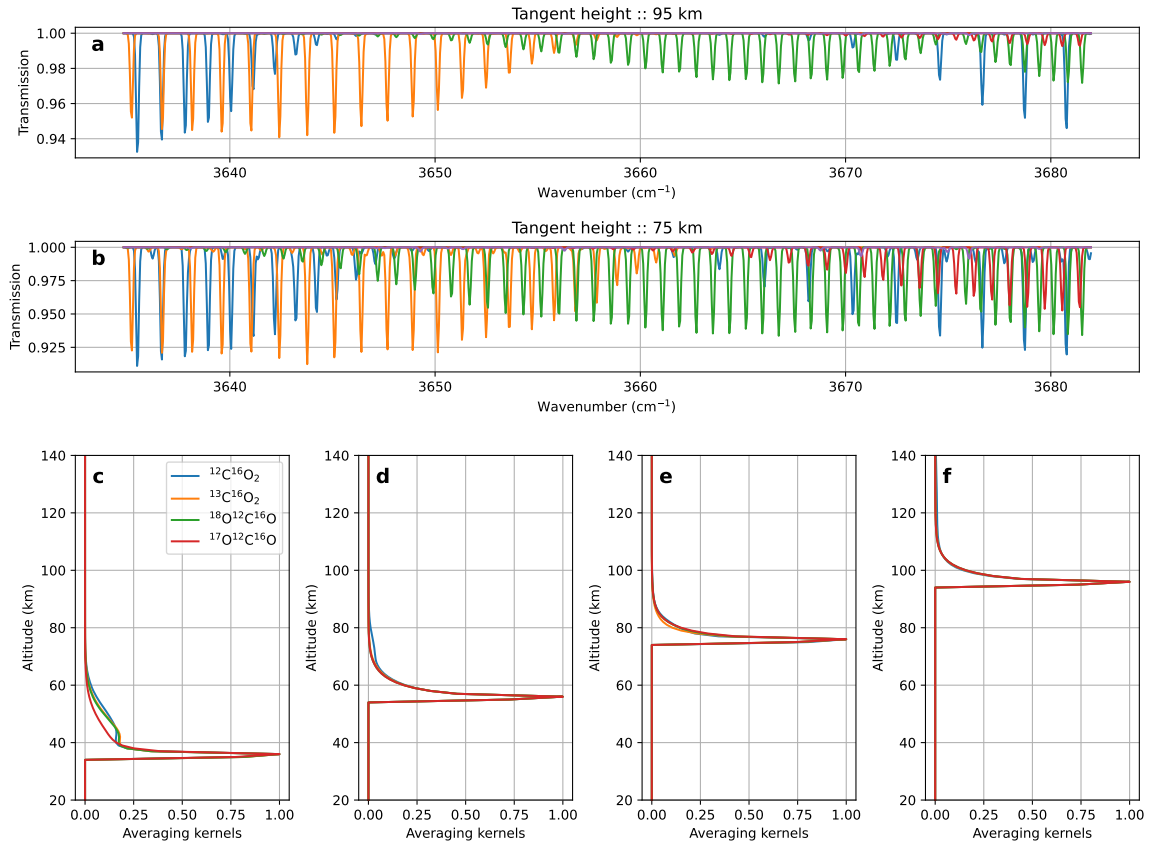


Figure 3. Sensitivity of the ACS MIR spectra along the line of sight. The top panels show two forward models at 95 (a) and 75 (b) km indicating the contribution of each isotopologue to the spectra. The bottom panels (c-f) show the normalised averaging kernels of the different isotopologues for a single measurement at tangent heights of 35, 55, 75 and 95 km, respectively. These kernels indicate that while below 70 km the contribution from layers above the tangent to the overall spectrum can be important and different for the several isotopologues, the kernels are narrower above 70 km and similar for the different isotopologues.

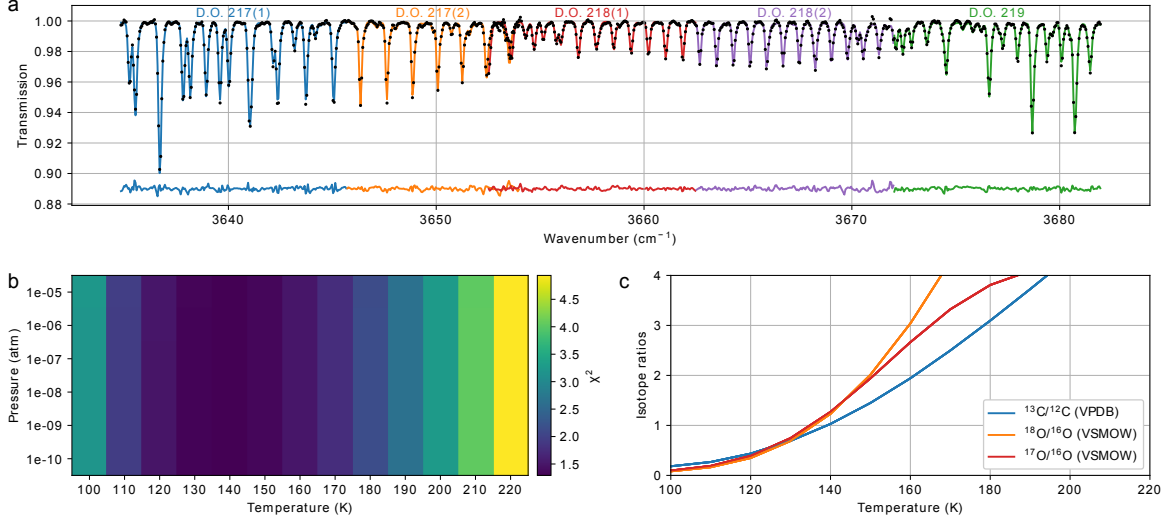


Figure 4. Sensitivity of the spectra and the derived isotopic ratios to the temperature. a) ACS MIR spectrum at 100 km made during orbit 1849 (black dots) and best fit to the data (coloured lines) when assuming a temperature of $T = 140$ K. The residuals between the best fit and the measured spectrum are also shown, with the colour of the lines highlighting the coverage of each of the spectral windows used for the retrieval. b) Reduced χ^2 achieved for the different cases of pressure and temperature. c) Derived isotopic ratios as a function of the assumed temperature.

ferent rows from the detector, which are later combined by means of a weighted average, as shown in Figure 5. In particular, the procedure used to derive the vertical profiles is summarised as follows:

1. For each solar occultation measurement, select all ACS MIR acquisitions above 70 km and retrieve the atmospheric temperature along with the line-of-sight densities of $^{12}\text{C}^{16}\text{O}_2$, $^{13}\text{C}^{16}\text{O}_2$, $^{18}\text{O}^{12}\text{C}^{16}\text{O}$ and $^{17}\text{O}^{12}\text{C}^{16}\text{O}$.
2. The isotopic ratios and the corresponding uncertainties are determined given the uncertainties in the line-of-sight densities of the different isotopologues, following

$$R = \frac{N_i}{N_1}, \quad (1)$$

$$\sigma_R = R \cdot \sqrt{\left(\frac{\sigma_{N_i}}{N_i}\right)^2 + \left(\frac{\sigma_{N_1}}{N_1}\right)^2}, \quad (2)$$

where N_1 represents the line-of-sight density of $^{12}\text{C}^{16}\text{O}_2$, and N_i represents the line-of-sight density of the other isotopologues of CO_2 .

3. Perform the retrieval and the derivation of the uncertainties introduced in the previous steps using six different detector rows, which allow the derivation of six vertical profiles for the atmospheric temperature and the isotopic ratios.
4. Combine the vertical profiles retrieved from each detector row by means of a weighted average given by

$$\bar{\mu}_j = \frac{\sum_{i=1}^6 \frac{x_{ij}}{\sigma_{ij}^2}}{\sum_{i=1}^6 \frac{1}{\sigma_{ij}^2}}, \quad (3)$$

266 where μ_j is the averaged profile at the j^{th} altitude level, and x_{ij} and σ_{ij}^2 are
 267 respectively the parameters (i.e., atmospheric temperature or isotopic ratios) and
 268 corresponding uncertainties derived for each detector row at each altitude level.
 269 5. The uncertainties associated with the averaged profile are calculated using

$$\bar{\sigma}_j = \text{Max} \left(\bar{\sigma}_1 = \sqrt{\frac{1}{\sum_{i=1}^6 \frac{1}{\sigma_{ij}^2}}} ; \bar{\sigma}_2 = \sqrt{\frac{\sum_{i=1}^6 \frac{(x_{ij} - \mu_j)^2}{\sigma_{ij}^2}}{\sum_{i=1}^6 \frac{1}{\sigma_{ij}^2}}} \right), \quad (4)$$

270 where the first term represents the standard error on the mean, derived from the
 271 propagation of errors from each of the retrieved profiles from each detector row,
 272 and the second term represents the standard deviation of these profiles around the
 273 mean. We consider this method for calculating the uncertainties to provide a more
 274 accurate representation of the true uncertainty of the retrieval in which not only
 275 the random uncertainties, but also the systematic ones are captured (e.g., effect
 276 of the doubling of the absorption lines, since it impacts each row of the detector
 277 differently, or the effect of the temperature in the retrieval of the isotopic ratios,
 278 since the retrieval from each row yields slightly different temperatures at each level).

279 In order to estimate the accuracy of the retrieval scheme, we perform a series of
 280 synthetic retrievals where the input isotopic ratios are known. These tests, explained more
 281 in-depth in Appendix A, reveal a very good accuracy of the retrievals of the $^{13}\text{C}/^{12}\text{C}$ ra-
 282 tio. On the other hand, these tests also reveal a bias in the retrieval of the O isotopic
 283 ratios: while the retrievals provide a good convergence at the lowermost altitudes (~ 70
 284 km), the retrieved O isotope ratios are on average systematically higher (~ 0.05 VSMOW)
 285 than those used to generate the synthetic spectra near 100 km. This bias can lead to an
 286 unreal increase of the O isotope ratios with altitude, which must be taken into account
 287 when analysing the retrieved ratios (see Figures 5 and A1).

288 4 Results

289 The retrieval scheme introduced in the previous section is applied to all available
 290 secondary grating position 4 full-frame observations made by ACS MIR from March 2018
 291 to February 2021 (see Figure 2). The results from this analysis are summarised in Fig-
 292 ure 6, which shows the climatology of the retrieved atmospheric parameters. In the fol-
 293 lowing subsections, these results are analysed in more detail in order to highlight aspects
 294 of the data aiming to understand the variability of the isotopic ratios, the average val-
 295 ues representative of the present-day atmosphere and the implications of these measure-
 296 ments to our understanding of the evolution of the Martian atmosphere throughout his-
 297 tory.

298 4.1 Variability of the Isotopic Ratios

299 The evolution of the retrieved parameters with solar longitude in Figure 6 shows
 300 variations above the level of measured uncertainties, suggesting that these variations are
 301 not caused by the statistical error of the measurements, but by real processes in the at-
 302 mosphere. We find the isotopic ratios to vary most noticeably as a function of altitude,
 303 showing repeatable patterns of variation throughout most of the observed period. Fig-
 304 ure 7 shows the retrieved vertical profiles of temperature and the isotopic ratios mea-
 305 sured in this dataset, as well as the averaged profiles from these, which represent the al-
 306 titude trends between 70 and 130 km. We identify two main features in the altitude trends
 307 of the isotopic ratios: an increase in the O isotopic ratios from 70 to 100 km, and a de-
 308 crease in the $^{13}\text{C}/^{12}\text{C}$ and $^{18}\text{O}/^{16}\text{O}$ isotopic ratios above ~ 100 km.

309 The averaged profiles of the O isotopic ratios in Figure 7 show a significant increase
 310 from 0.9-1.0 VSMOW at 70-80 km, to 1.0-1.1 VSMOW at 95-105 km. This increase ap-

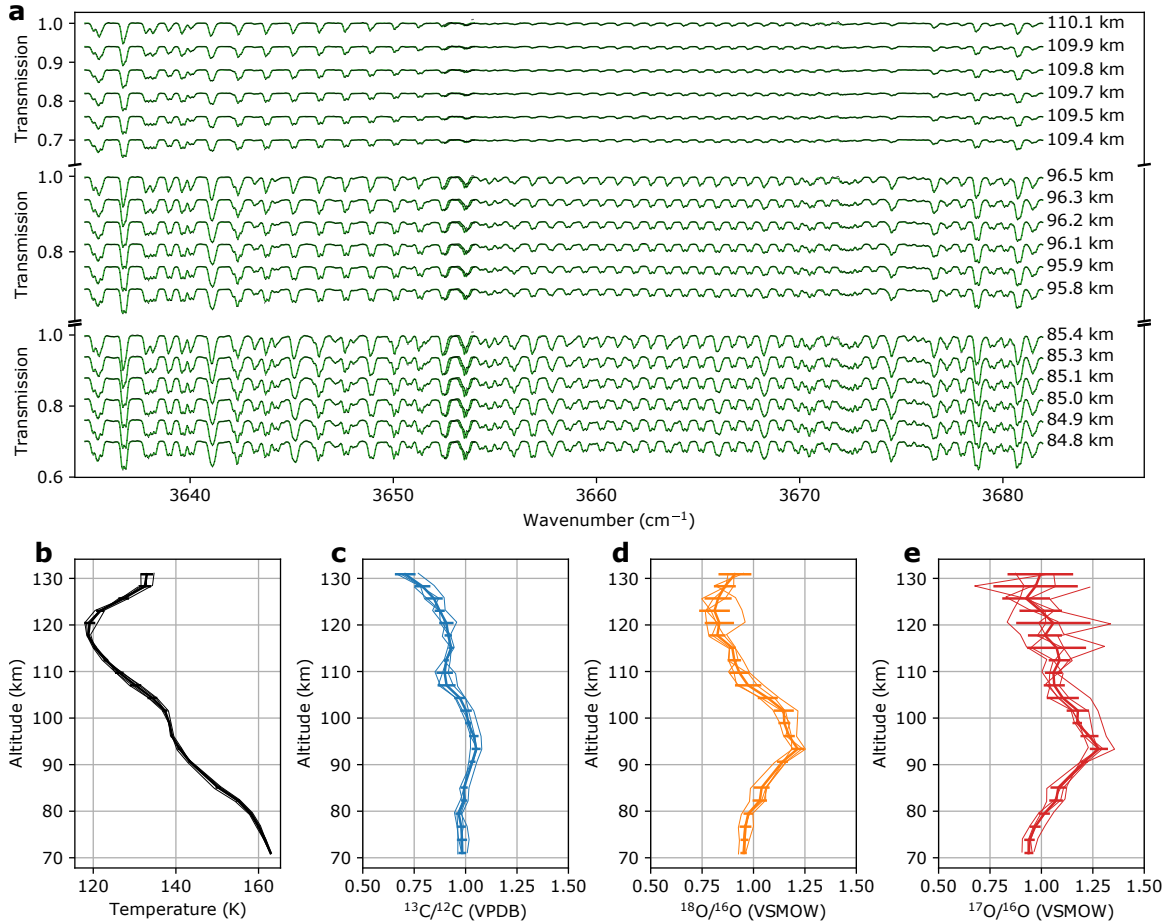


Figure 5. Example of ACS MIR spectra and summary of retrieval scheme. ACS MIR spectra shown in this figure (a) were obtained during the solar occultation in orbit 1849 (Latitude = 82°, $L_S = 163^\circ$ in MY34, Local time = 3h). Retrievals of the rotational temperature (b) and the line-of-sight densities of $^{12}\text{C}^{16}\text{O}_2$, $^{13}\text{C}^{16}\text{O}_2$, $^{18}\text{O}^{12}\text{C}^{16}\text{O}$, $^{17}\text{O}^{12}\text{C}^{16}\text{O}$ are performed independently using spectra from six different rows from the detector, which allow the derivation of the $^{13}\text{C}/^{12}\text{C}$ (c), $^{18}\text{O}/^{16}\text{O}$ (d) and $^{17}\text{O}/^{16}\text{O}$ (e) isotopic ratios. The retrieved profiles from each of the detector rows (thin lines) are later combined by means of a weighted average (thick lines). The increase in the $^{18}\text{O}/^{16}\text{O}$ and $^{17}\text{O}/^{16}\text{O}$ isotopic ratios is caused by a systematic bias in the retrieval scheme, which must be taken into account when analysing the variations of the isotopic ratios.

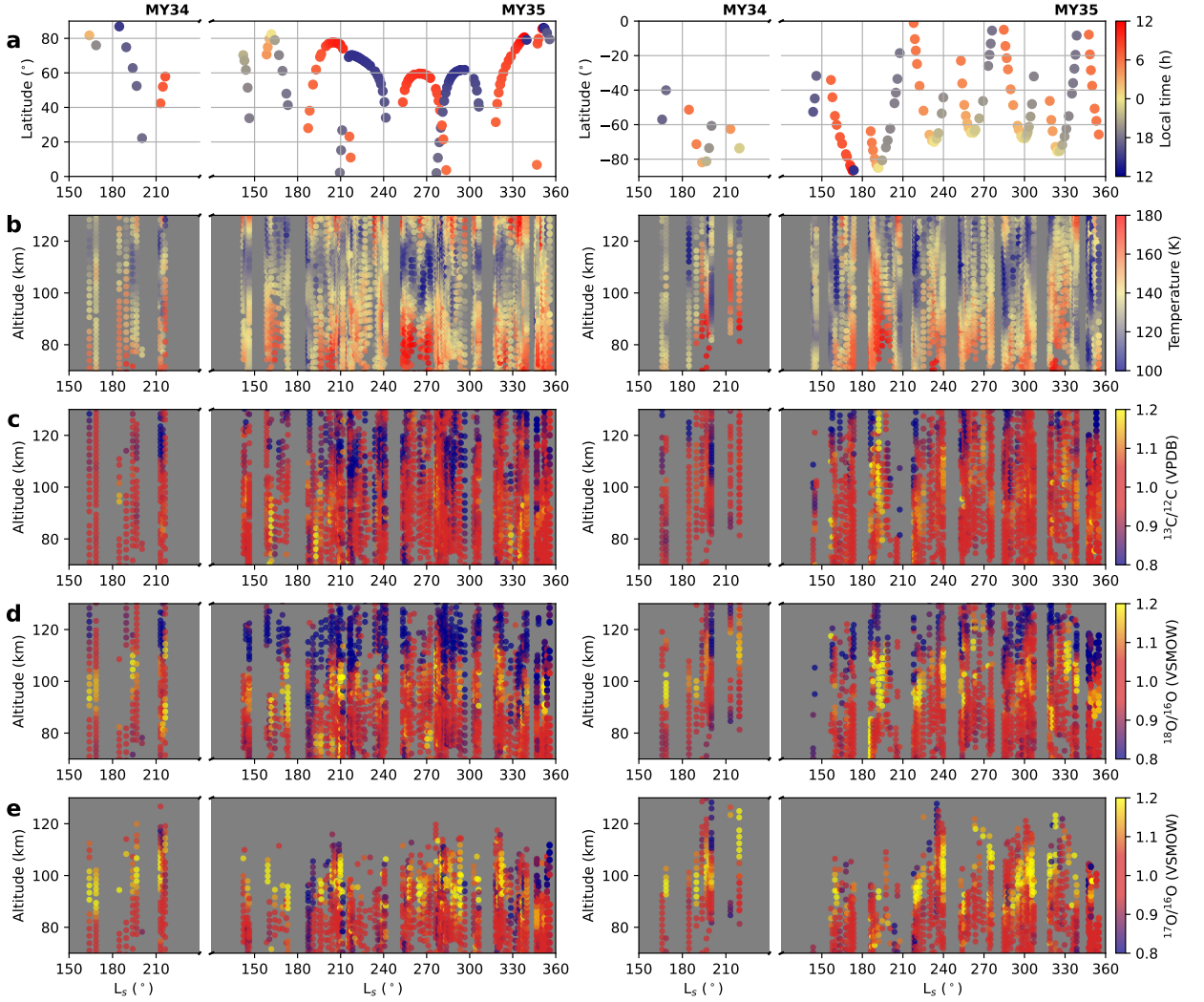


Figure 6. Climatology of the retrieved atmospheric parameters. The panels show the values of the retrieved parameters as a function of altitude and solar longitude for the northern (left) and southern (right) hemispheres. The panels in each of the rows represent the distribution of ACS MIR solar occultation observations, with the local time represented by the colour bar (a), the atmospheric temperature (b), and the $^{13}\text{C}/^{12}\text{C}$ (c), $^{18}\text{O}/^{16}\text{O}$ (d) and $^{17}\text{O}/^{16}\text{O}$ (e) isotopic ratios with uncertainties lower than 0.075 VPDB or VSMOW. Most noticeable variations of the isotopic ratios are observed to occur as a function of altitude. To first order, no discernible patterns of variations are identified as a function of latitude, solar longitude or local time.

311 appears not to be followed by the $^{13}\text{C}/^{12}\text{C}$ isotopic ratio, which remains constant through-
 312 out this altitude range. An enrichment in the isotopic ratios of CO_2 could happen due
 313 to the difference in the ultraviolet photolysis cross-sections of the different isotopologues:
 314 the cross-sections of the heavy isotopes of carbon dioxide are smaller than those of the
 315 main isotopologue, which would therefore deplete the photolysis products in the heavy
 316 isotopes, leaving the unphotolysed CO_2 relatively enriched in these (Schmidt et al., 2013).
 317 However, based on the calculations by Schmidt et al. (2013), photolysis would prefer-
 318 entially enrich the $^{13}\text{C}/^{12}\text{C}$ ratio over both oxygen ratios, which is not what is inferred
 319 from the observations.

320 A systematic bias in the retrieved O isotopic ratios with altitude was identified while
 321 validating the retrieval scheme against synthetic spectra (see Appendix A). In particu-
 322 lar, the retrieved O isotopic ratios were found to be increasingly overestimated with alti-
 323 tude, while the $^{13}\text{C}/^{12}\text{C}$ ratio was found to converge at all altitudes. This systematic
 324 bias, which is most likely caused by the simplified radiative transfer calculations used
 325 in this study, which assume a constant temperature along the path, is expected to oc-
 326 cur in the ACS MIR observations too. Therefore, we conclude that the increase observed
 327 in the $^{18}\text{O}/^{16}\text{O}$ and $^{17}\text{O}/^{16}\text{O}$ is not caused by real fractionation, but by a systematic bias
 328 in the retrieval scheme.

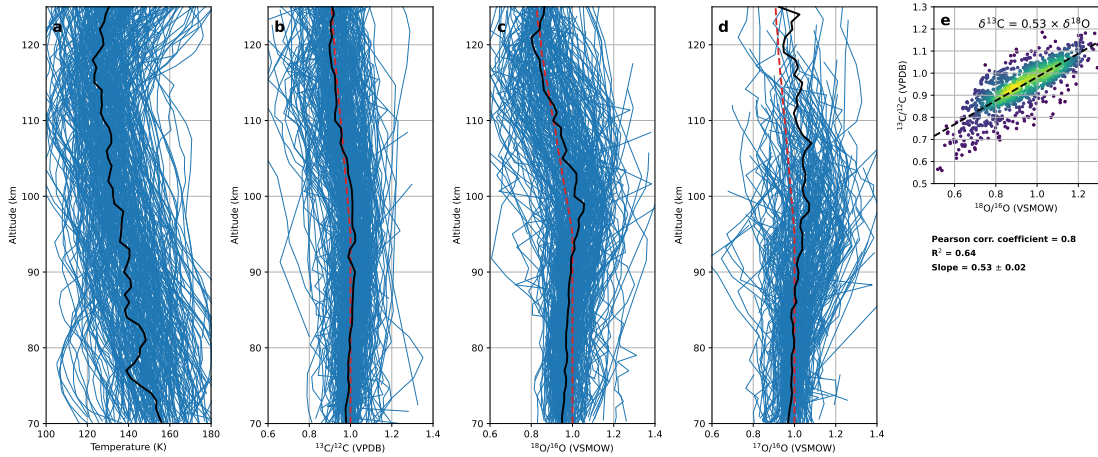


Figure 7. Heavy isotopes depleted with increasing altitude. The blue lines represent all measured vertical profiles of temperature (a), $^{13}\text{C}/^{12}\text{C}$ (b), $^{18}\text{O}/^{16}\text{O}$ (c) and $^{17}\text{O}/^{16}\text{O}$ (d) with uncertainties lower than 0.075 VPDB and VSMOW. Averaging these profiles allows the derivation of their altitude trends (black lines). The trends of the $^{18}\text{O}/^{16}\text{O}$ and $^{17}\text{O}/^{16}\text{O}$ isotopic ratios increase between 70 and 100 km, although this increase is caused by a systematic bias in the retrieval scheme. The trends of the $^{13}\text{C}/^{12}\text{C}$ and $^{18}\text{O}/^{16}\text{O}$ ratios show a decrease at the highest altitudes, consistent with the expectations of diffusive separation above the homopause altitude, which is located at $z_h = 95 \pm 2$ km. The correlation plot between the $^{13}\text{C}/^{12}\text{C}$ and $^{18}\text{O}/^{16}\text{O}$ ratios above 100 km (e) shows that the variations follow $\delta^{13}\text{C} \sim 0.5 \times \delta^{18}\text{O}$, consistent with the expectations from diffusive separation.

329 The altitude trends of the isotopic ratios in Figure 7 also show a decrease of the
 330 $^{13}\text{C}/^{12}\text{C}$ and $^{18}\text{O}/^{16}\text{O}$ isotopic ratios above an altitude of approximately 100 km. Be-
 331 low this altitude, the isotopic ratios are found to be essentially consistent with Earth-
 332 like fractionation. In the case of the $^{17}\text{O}/^{16}\text{O}$ ratio, although the measurements below
 333 100 km show a value consistent with Earth, there are fewer observations with low un-
 334 certainties above this altitude and the impact by the forementioned systematic bias keeps

335 increasing with altitude, which makes it difficult to conclude if this isotopic ratio also
 336 decreases (see Figure A1). A decrease in the isotopic ratios at these altitudes follows the
 337 expectations from diffusive separation, which predict the density of each isotopologue
 338 to decrease according to their own mass-dependent scale heights above the homopause
 339 (e.g., Jakosky et al., 1994). The decrease of the isotopic ratios above the homopause due
 340 to diffusive separation is therefore established by the ratio of densities of the different
 341 isotopologues as a function of altitude and is given by

$$R(z) = R_h \cdot \exp\left(\frac{-\Delta m \cdot g \cdot (z - z_h)}{k_B \cdot T}\right), \quad (5)$$

342 where R_h represents the isotopic ratio at the homopause, Δm is the mass differ-
 343 ence between the two isotopologues (1 a.m.u for $^{13}\text{C}/^{12}\text{C}$ and $^{17}\text{O}/^{16}\text{O}$, and 2 a.m.u for
 344 $^{18}\text{O}/^{16}\text{O}$), g is the gravitational acceleration at the modelled altitude, z_h is the altitude
 345 of the homopause, k_B is Boltzmann's constant, and T is the temperature (e.g., Jakosky
 346 et al., 1994).

347 In order to estimate the homopause altitude z_h from the observations of the iso-
 348 topic ratios, the model for diffusive separation in equation 5 is fit to the averaged $^{13}\text{C}/^{12}\text{C}$
 349 profile, using the measured temperature profile and assuming Earth-like fractionation
 350 below the homopause. The best fit, also displayed in Figure 7, shows a good agreement
 351 with the data, in which the retrieved homopause altitude was found to be $z_h = 95 \pm 2$
 352 km. Slipski et al. (2018) monitored the altitude of the homopause in different seasons,
 353 local times and locations using the ratio of N_2 to Ar densities measured by NGIMS on-
 354 board the MAVEN spacecraft. These results show that the homopause is typically set
 355 at altitudes between 90 and 110 km, which agrees with the altitude at which we observe
 356 the fractionation.

357 While the altitude trend of the $^{18}\text{O}/^{16}\text{O}$ ratio also shows a decrease above ~ 100
 358 km, it shows a poorer agreement with the model for diffusive separation, most likely due
 359 to the systematic bias mentioned before (see Figure 7c). Another way of unravelling the
 360 nature of the observed fractionation and test whether the decrease in the $^{13}\text{C}/^{12}\text{C}$ and
 361 $^{18}\text{O}/^{16}\text{O}$ ratios is caused by diffusive separation is to look at the correlation plots be-
 362 tween these. Fractionation due to diffusive separation occurs because of the slightly dif-
 363 ferent mass of the several isotopologues, which requires the variations of the isotope ra-
 364 tios to follow the expectations from mass-dependent fractionation (i.e., $\delta^{13}\text{C} \sim 0.5 \times \delta^{18}\text{O}$)
 365 (Young et al., 2002). Panel E on Figure 7 shows the correlation between the measured
 366 $^{13}\text{C}/^{12}\text{C}$ and $^{18}\text{O}/^{16}\text{O}$ ratios above 100 km, which show a positive linear correlation with
 367 a Pearson correlation coefficient of 0.8. In order to calculate the slope of the correlation
 368 we perform a linear regression which suggests that the measurements follow fractiona-
 369 tion given by $\delta^{13}\text{C} = (0.53 \pm 0.02) \times \delta^{18}\text{O}$, which is in agreement with the expectations
 370 from mass-dependent fractionation. While the forementioned systematic bias is expected
 371 to produce an overestimation of the $^{18}\text{O}/^{16}\text{O}$ isotopic ratios, this is expected to be ap-
 372 proximately constant in this altitude range, which does not affect the slope of the rela-
 373 tion between $\delta^{13}\text{C}$ and $\delta^{18}\text{O}$. Therefore, we conclude that the observed decrease in the
 374 isotopic ratios is caused by diffusive separation of the different isotopologues above the
 375 homopause.

376 Apart from the variations of the isotopic ratios as a function of altitude, the ACS
 377 dataset allows the analysis of potential seasonal and latitudinal variations. To first or-
 378 der, we find no differences in the behaviour of the isotopic ratios as a function of lati-
 379 tude, season or local time, which show similar altitudinal patterns throughout most of
 380 the observed period. The altitude of the homopause varies as a function of L_S , latitude
 381 and local time, which will therefore produce variations of the minimum altitude at which
 382 the isotope ratios fractionate due to diffusive separation (Slipski et al., 2018). Similarly,
 383 Livengood et al. (2020) found variations of the $^{18}\text{O}/^{16}\text{O}$ ratio with local time and sur-

face temperature, which appear to be caused by surface-atmosphere interactions. However, given the uncertainties of the derived profiles from this dataset, we find no statistically significant differences between the profiles in both hemispheres, different local times, or in different periods of L_S .

4.2 Average Isotopic Ratios in the Present-day Atmosphere

Estimations of the average isotopic ratios in CO_2 are essential for our understanding of the evolution of the atmosphere of Mars throughout history. Isotopic ratios inferred from localised measurements are subject to climatological processes that might affect the isotopic composition of the sample. In order to estimate the isotopic ratios representative of the Martian atmospheric reservoir, one must disentangle the values inferred from these measurements from potential sources of fractionation occurring in the atmosphere.

Figure 8 shows a histogram of the measured isotopic ratios in CO_2 as well as their corresponding uncertainties. The histograms are separated in three altitude regions (70-90 km; 90-110 km; 110-130 km), which can be used to disentangle the points affected by fractionation (e.g., diffusive separation). The histograms show that most of the points with uncertainties lower than 75‰ correspond to the measurements between 70 and 90 km. The average values from the measurements made in this altitude range are $^{13}\text{C}/^{12}\text{C} = 0.997 \pm 0.037$ VPDB, $^{18}\text{O}/^{16}\text{O} = 0.971 \pm 0.038$ VSMOW and $^{17}\text{O}/^{16}\text{O} = 0.989 \pm 0.041$ VSMOW (i.e., $\delta^{13}\text{C} = -3 \pm 37$ ‰, $\delta^{18}\text{O} = -29 \pm 38$ ‰ and $\delta^{17}\text{O} = -11 \pm 41$ ‰), where the uncertainties correspond to the average measurement uncertainties (see Figure 8). While the measurements of $^{13}\text{C}/^{12}\text{C}$ between 90 and 110 km follow a distribution similar to that observed between 70 and 90 km, the measurements of $^{18}\text{O}/^{16}\text{O}$ and $^{17}\text{O}/^{16}\text{O}$ show more variability, partly caused by the greater typical uncertainties in this altitude range, and a higher mean value, caused by the systematic bias in the retrievals of these ratios, which tends to overestimate the isotopic ratios at these altitudes (see Figure A1). It must be noted that the histograms in the 70-90 km range might also include a slight overestimation of the O isotopic ratios due to this systematic bias. However, the variability of the slightly increasing trends of $^{18}\text{O}/^{16}\text{O}$ and $^{17}\text{O}/^{16}\text{O}$ in this altitude range are well covered by the reported uncertainties. Lastly, the measurements of the $^{13}\text{C}/^{12}\text{C}$ and $^{18}\text{O}/^{16}\text{O}$ isotopic ratios between 110 and 130 km depict values significantly smaller than those measured at lower altitudes due to the presence of fractionation above the homopause (see Figure 7).

Taking into account the accuracy of the retrievals and the variations of the isotopic ratios discussed in the previous sections, we consider the values measured in the lowest altitude range (70-90 km) to represent the average isotopic ratios representative of CO_2 in the atmosphere of Mars. These values may be compared with those reported in other studies (see Table 1). In particular, special attention is given to the comparison with the measurements from the Curiosity Rover (Webster et al., 2013), which show the lowest uncertainties and are often used as the isotopic ratios representative of the present-day Martian atmosphere in evolutionary models (Hu et al., 2015; Jakosky, 2019). The measurements of Webster et al. (2013) revealed an enrichment in the heavy isotopes of carbon dioxide with respect to Earth-like fractionation ($\delta^{13}\text{C} = 46 \pm 4$ ‰; $\delta^{18}\text{O} = 48 \pm 5$ ‰; $\delta^{17}\text{O} = 24 \pm 5$ ‰). While these results are nominally consistent with our measurements, our derived average isotopic ratios do not show any evidence of enrichment in the heavy isotopes with respect to Earth.

One possible scenario to reconcile both measurements by SAM/TLS and ACS requires the presence of isotopic fractionation between the lower and upper atmospheres of Mars: while the Curiosity Rover measures the isotopic ratios on the surface, the analysis presented in this study is performed using observations between 70 and 130 km. However, it is not clear which processes could generate a depletion in the isotopic ratios between the lower and upper atmospheres of Mars. Condensation of CO_2 into ice clouds

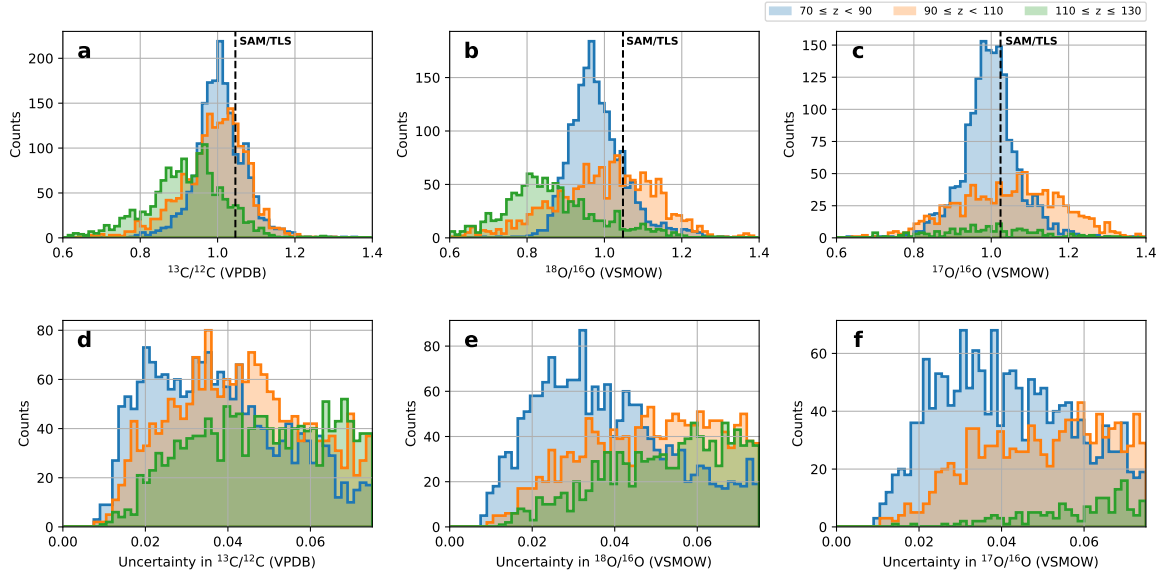


Figure 8. Histograms of the measured $^{13}\text{C}/^{12}\text{C}$ (a), $^{18}\text{O}/^{16}\text{O}$ (b) and $^{17}\text{O}/^{16}\text{O}$ (c) isotopic ratios and their retrieved uncertainties (d,e,f). The histograms for the different isotopic ratios are separated in three altitude regions (70-90 km - blue; 90-110 km - orange; 110-130 km - green) to highlight the variability of the vertical structure of the isotopic ratios. The black dashed lines in panels a,b and c represent the values of the isotopic ratios reported by Webster et al. (2013).

Table 1. Measured isotope ratios in CO_2 compared to previous studies, expressed as a deviation with respect to the VPDB and VSMOW standards, which are representative of Earth-like fractionation.

Reference	Method	$\delta^{13}\text{C}$ (‰)	$\delta^{18}\text{O}$ (‰)	$\delta^{17}\text{O}$ (‰)
Schrey et al. (1986)	Earth-based	-73 ± 58	-37 ± 121	-
Owen (1982)	Viking Lander	-11 ± 55	-2 ± 50	-
Krasnopolsky et al. (1996)	Earth-based	-60 ± 150	-130 ± 80	-
Encrenaz et al. (2005)	Earth-based	0 ± 110	-	-
Krasnopolsky et al. (2007)	Earth-based	-22 ± 20	18 ± 18	-
Niles et al. (2010)	Phoenix Lander	-2.5 ± 4.3	31.0 ± 5.7	-
Webster et al. (2013)	Curiosity Rover	46 ± 4	48 ± 5	24 ± 5
Livengood et al. (2020)	Earth-based	-	9 ± 14	-
This study	ACS/TGO	-3 ± 37	-29 ± 38	-11 ± 41

435 preferentially depletes the atmosphere in the heavy isotopes, although the magnitude of
 436 this depletion is expected to be small, especially for the carbon isotopic ratio, which may
 437 actually enrich the atmosphere in ^{13}C (Eiler et al., 2000). In addition, while formation
 438 of CO_2 ice clouds occurs sporadically in the atmosphere of Mars, the ACS measurements
 439 extend over a large range of latitudes, seasons and local times, which makes it unlikely
 440 that the isotopic ratios can be continuously fractionated by this mechanism. Another
 441 mechanism potentially depleting the isotopic ratios with altitude is the diffusive separa-
 442 tion of the different isotopologues above the homopause, which is set at altitudes of
 443 approximately 100 km (see Figure 7 and Slipski et al. (2018)). However, our derivation
 444 of the average isotopic ratios is performed using measurements between 70 and 90 km,
 445 where diffusive separation is not expected to continuously fractionate the isotopic ratios.

446 Another possible scenario that might explain the differences between SAM/TLS
 447 and ACS lies on the impact of climatological isotopic fractionation in the derivation of
 448 the averaged isotopic ratios from both datasets. The ACS measurements extend over a
 449 large range of locations, seasons and local times, which allows averaging over hundreds
 450 of measurements, from which the effects of climatological fractionation are expected to
 451 be small. In that sense, although the measurements made by the Curiosity Rover are more
 452 precise, they were always made in the same location, at roughly the same local time, and
 453 covering only about 10% of a full Martian year. The contribution from seasonal cycling
 454 to these measurements is unknown, and so they might therefore not be representative
 455 of the whole atmospheric reservoir. In fact, Livengood et al. (2020) revealed high vari-
 456 ability of the $^{18}\text{O}/^{16}\text{O}$ in the near-surface atmosphere, varying from $\delta^{18}\text{O} = -92 \pm 23$
 457 ‰ to $\delta^{18}\text{O} = 71 \pm 18$ ‰ over a temperature increase from 266.9 to 275.4 K, which is
 458 most likely caused by surface-atmosphere interactions. On average, the measurements
 459 reported by Livengood et al. (2020) are essentially consistent with Earth-like fractiona-
 460 tion (see Table 1). In addition, the values derived from different studies are in some cases
 461 inconsistent within the reported uncertainties, which might be indicative of isotopic frac-
 462 tionation in the atmosphere.

463 4.3 Implications to the Evolution of Mars' Atmosphere

464 Comparison between the primordial isotopic ratios and those in the present-day
 465 atmosphere allow the estimation of the amount of atmosphere lost to space throughout
 466 history. In particular, considering that CO_2 constitutes the major reservoir of C in the
 467 Martian atmosphere, the $^{13}\text{C}/^{12}\text{C}$ ratio allows the estimation of the amount of CO_2 lost
 468 to space assuming Rayleigh distillation, which is given by

$$R = R_0 \cdot x^{f-1}, \quad (6)$$

469 where R and R_0 represent the present-day and primordial $^{13}\text{C}/^{12}\text{C}$ ratio, respec-
 470 tively, x is the fraction of remaining atmosphere and f is the fractionation factor, which
 471 determines the efficiency of escape of the heavy isotope with respect to that of the lighter
 472 one. In particular, the fractionation factor is defined as

$$f = \frac{\phi_{^{13}\text{C}}/\phi_{^{12}\text{C}}}{(^{13}\text{C}/^{12}\text{C})_s}, \quad (7)$$

473 where $\phi_{^{12}\text{C}}$ and $\phi_{^{13}\text{C}}$ are the fluxes of escaping atoms of the two isotopologues, and
 474 $(^{13}\text{C}/^{12}\text{C})_s$ is the isotopic ratio representative of the near-surface atmospheric reservoir.

475 Based on a primordial isotopic composition from measurements of magmatic car-
 476 bon from Martian meteorites ($\delta^{13}\text{C} = -(20-30)$ ‰; Wright et al., 1986) and the isotopic
 477 composition of CO_2 in the present-day atmosphere measured by the Curiosity Rover ($\delta^{13}\text{C}$
 478 = 46 ‰; Webster et al., 2013), Jakosky (2019) estimated that at least 50% of the C reser-

voir has been lost to space throughout time. This estimation relies on the assumption that a substantial part of C was lost to space due to sputtering by pickup ions, where the fractionation factor is given by diffusive separation between the homopause and exobase altitudes (see equation 1). Jakosky (2019) estimated the escape fractionation factor of $^{13}\text{C}/^{12}\text{C}$ using the analogue factor derived by Jakosky et al. (2017) for the $^{38}\text{Ar}/^{36}\text{Ar}$ ratio using measurements from the MAVEN spacecraft, and re-scaling it taking into account the mass difference of 1 a.m.u for the C isotopes as compared to the 2 a.m.u for the isotopes of Ar. Based on these calculations, the average fractionation factor between the homopause and exobase altitudes due to diffusive separation is estimated to be $f_{h-e} \sim 0.9$. The main goal of this section is to apply the same approach as that of Jakosky (2019), but considering the implications of the $^{13}\text{C}/^{12}\text{C}$ measurements by ACS reported in this study. In particular, we consider the two suggested scenarios to reconcile the datasets between ACS and SAM/TLS.

In the first scenario, the difference between the average isotopic ratios derived from the ACS and SAM/TLS datasets implies a continuous source of fractionation between the isotopic ratios at the surface ($\delta^{13}\text{C} = 46 \text{ ‰}$) and the homopause ($\delta^{13}\text{C} = -3 \text{ ‰}$), which must be accounted for in the estimation of the fractionation factor. In particular, the net fractionation factor in this scenario is given by

$$f = f_{s-h} \cdot f_{h-e}, \quad (8)$$

where f_{h-e} is the fractionation factor between the exobase and the homopause due to diffusive separation determined by Jakosky (2019) ($f_{h-e} \sim 0.9$) and f_{s-h} is the fractionation factor between the homopause and the surface ($f_{s-h} = (^{13}\text{C}/^{12}\text{C})_h / (^{13}\text{C}/^{12}\text{C})_s = 0.997/1.046 = 0.953$). Including this overall fractionation factor in the Rayleigh distillation equation (see equation 6), and assuming that the isotopic ratio representative of the present-day atmosphere is that measured by the Curiosity Rover, we estimate that at least 40% of C in the Martian atmosphere has escaped to space throughout history (see Figure 9).

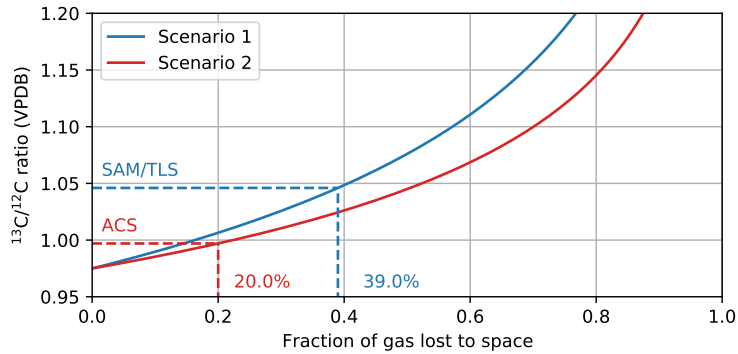


Figure 9. Estimation of the fraction of C lost to space throughout history from the $^{13}\text{C}/^{12}\text{C}$ isotopic ratio assuming Rayleigh distillation. In the first scenario, the isotopic composition of CO_2 is assumed to follow the measurements by SAM/TLS, but considering fractionation between the lower atmosphere and the homopause. In the second scenario, the isotopic composition of CO_2 is assumed to follow the measurements by ACS, with no fractionation between the lower atmosphere and the homopause. In both scenarios the fractionation above the homopause is assumed to be caused by diffusive separation.

505 In the second scenario, we assume that the $^{13}\text{C}/^{12}\text{C}$ representative of the Martian
 506 atmospheric reservoir follows the value derived from the ACS dataset. In this case, the
 507 enrichment in the heavy isotope with respect to the standard measured by Webster et
 508 al. (2013) is considered to be representative of the Martian atmosphere at a particular
 509 time and location impacted by climatological fractionation, but not representative of the
 510 atmospheric reservoir as a whole. Using the fractionation factor between the homopause
 511 and exobase altitudes due to diffusive separation ($f = f_{h-e} \sim 0.9$), we estimate that at
 512 least 20% of C in the Martian atmosphere has escaped to space throughout history (see
 513 Figure 9).

514 While these calculations provide a first-order estimate of the amount of C lost to
 515 space through time, a more accurate estimation of this quantity requires the combina-
 516 tion of the several mechanisms by which C escapes to space and their corresponding frac-
 517 tionation factors. Early studies suggested the main source of C escape to be the disso-
 518 ciative recombination of CO^+ (McElroy, 1972), although further analyses revealed that
 519 it is the photodissociation of CO molecules that is the dominant process for the produc-
 520 tion of escaping C on Mars (Fox & Bakalian, 2001; Grller et al., 2014; Cui et al., 2019).
 521 The escape fractionation factors by the photodissociation of CO (Hu et al., 2015) and
 522 the dissociative recombination of CO^+ (Fox & Ha, 1999) are lower than the fractiona-
 523 tion factor induced by sputtering. In this case, the atmosphere would get more efficiently
 524 enriched in the heavy isotope as it escapes to space, indicating that a lower fraction of
 525 C would have been lost from the atmosphere of Mars through time. However, as noted
 526 by Jakosky (2019), the estimations performed in this study provide a lower limit on the
 527 amount of atmospheric escape, since other processes such as carbonate formation or out-
 528 gassing of gas from the interior would result in a relative depletion of the heavy isotope
 529 in the atmosphere.

530 4.4 Relation between the O Isotope Composition of H_2O and CO_2

531 Fractionation between the isotopic composition of H_2O and CO_2 will result if oxy-
 532 gen is exchanging between them. Therefore, examining the relative $\delta^{18}\text{O}$ can provide an
 533 insight on how these species interact with each other. The isotopic composition of H_2O
 534 in the Martian atmosphere was reported by Alday et al. (2021) using ACS MIR solar
 535 occultation observations also made with secondary grating position 4. This analysis re-
 536 vealed an average non-fractionated isotopic ratio of $^{18}\text{O}/^{16}\text{O}$ (H_2O) = 1.140 ± 0.080 VS-
 537 MOW ($\delta^{18}\text{O}$ (H_2O) = 140 ± 80 ‰), which is therefore more enriched in the heavy iso-
 538 tope than that in CO_2 ($\delta^{18}\text{O}$ (CO_2) = -29 ± 38 ‰). Although the altitude regions where
 539 the isotopes of H_2O and CO_2 were measured with ACS MIR are different (10-50 km for
 540 H_2O and 70-130 km for CO_2), which might impede a direct comparison between these,
 541 the measurements by SAM/TLS at the surface reported by Webster et al. (2013) also
 542 indicate a higher enrichment of H_2O in the heavy isotopes compared to CO_2 ($\delta^{18}\text{O}$ (H_2O)
 543 = 84 ± 10 ‰ and $\delta^{18}\text{O}$ (CO_2) = 48 ± 5 ‰).

544 Based on the equilibrium fractionation of ^{18}O between CO_2 and H_2O derived by
 545 Urey (1947) from their different binding energies, Jakosky (1991) suggested that $\delta^{18}\text{O}$
 546 should be approximately 80‰ higher in CO_2 than that in H_2O on Mars. This equilib-
 547 rium could be reached if for example liquid water was present in the near-surface layer,
 548 where CO_2 would be dissolved and would quickly exchange oxygen isotopes with the wa-
 549 ter. With the liquid water then exchanging with the gases in the atmosphere, the dif-
 550 ferent oxygen-bearing species in the atmosphere would also reflect this equilibrium frac-
 551 tionation (Jakosky, 1991). Although liquid water is unstable under the present Martian
 552 conditions, it can be present occasionally as a transient phase (Martn-Torres et al., 2015).
 553 However, based on the measured isotope composition in both species, this type of equi-
 554 librium does not appear to be dominant in the Martian atmosphere.

555 Instead, oxygen might be exchanged by photochemical reactions that may ultimately
 556 lead to the preferential transfer of certain isotopes to a given species. One pathway by
 557 which oxygen is transferred from H_2O to CO_2 starts with the photodissociation of H_2O
 558 into OH ($\text{H}_2\text{O} + h\nu \rightarrow \text{OH} + \text{H}$). This newly formed odd-hydrogen will later on recom-
 559 bine with CO , giving rise to CO_2 ($\text{CO} + \text{OH} \rightarrow \text{CO}_2 + \text{H}$) (McElroy & Donahue, 1972).
 560 Based on the differential photolysis cross sections of H_2^{16}O and H_2^{18}O (Miller & Yung,
 561 2000), Alday et al. (2021) estimated that the $^{18}\text{O}/^{16}\text{O}$ isotopic ratio of the formed OH
 562 molecules would be approximately 0.975 times lower than that of the parent H_2O molecules.
 563 The recombination of the OH molecules into CO_2 might therefore result in the trans-
 564 fer of oxygen depleted in ^{18}O from H_2O to CO_2 .

565 5 Summary

566 Transmission spectra acquired by the Atmospheric Chemistry Suite on the Exo-
 567 Mars Trace Gas Orbiter allow the monitoring of the C and O isotopic ratios in CO_2 in
 568 the atmosphere of Mars. In this study, we develop a retrieval scheme to simultaneously
 569 retrieve the isotopic ratios along with the rotational temperature of CO_2 , which is found
 570 to be essential for an accurate characterisation of the isotopic ratios. This retrieval scheme
 571 is applied to all ACS MIR observations made with secondary grating position 4 between
 572 70 and 130 km. The observational coverage is divided in two periods, one covering the
 573 range $L_S = 164\text{-}219^\circ$ in Martian year 34 (MY34), and the second one covering the range
 574 $L_S = 141\text{-}356^\circ$ in MY35.

575 Averaging the retrieved profiles of the isotopic ratios allow the analysis of their alti-
 576 tude trends, which show two main patterns of variations. One pattern comprises an
 577 increase in the $^{18}\text{O}/^{16}\text{O}$ and $^{17}\text{O}/^{16}\text{O}$ isotopic ratios from 0.9-1.0 VSMOW at 70-80 km,
 578 to 1.0-1.1 VSMOW at 95-105 km, not followed by the $^{13}\text{C}/^{12}\text{C}$ ratio. However, a series
 579 of tests using synthetic spectra revealed a systematic overestimation of the O isotopic
 580 ratios with altitude, consistent with the increase with altitude observed in the dataset.
 581 Therefore, we conclude that the observed increase in the O isotopic ratios is not caused
 582 by real atmospheric fractionation, but by a systematic bias in the retrieval scheme. The
 583 second pattern of variations comprise a decrease of the $^{13}\text{C}/^{12}\text{C}$ and $^{18}\text{O}/^{16}\text{O}$ isotopic
 584 ratios above an altitude of approximately 100 km, which is consistent with the expect-
 585 ations from fractionation above the homopause due to diffusive separation. In partic-
 586 ular, fitting the model of this source of fractionation to the vertical trends of the $^{13}\text{C}/^{12}\text{C}$
 587 ratio reveals a homopause altitude of $z_h = 95 \pm 2$ km, consistent with the values observed
 588 in other studies (Slipski et al., 2018).

589 Making use of the statistics from whole ACS dataset, we derive the isotopic ratios
 590 representative of CO_2 in the present-day atmospheric reservoir outside of fractionation
 591 ($\delta^{13}\text{C} = -3 \pm 37$ ‰; $\delta^{18}\text{O} = -29 \pm 38$ ‰; $\delta^{17}\text{O} = -11 \pm 41$ ‰). These values differ from
 592 those measured by SAM/TLS on the Curiosity Rover (Webster et al., 2013), which were
 593 found to be enriched in the heavy isotopes with respect to the standard Earth-like rat-
 594 ios ($\delta^{13}\text{C} = 46 \pm 4$ ‰; $\delta^{18}\text{O} = 48 \pm 5$ ‰; $\delta^{17}\text{O} = 24 \pm 5$ ‰). In order to reconcile the
 595 measurements from both instruments, we propose two possible scenarios. The first sce-
 596 nario considers the difference between the derived average values to arise from a contin-
 597 uous source of fractionation between the lower and upper atmospheres of Mars, which
 598 needs to be accounted for if estimating the escape fractionation factor. In the second sce-
 599 nario, we consider the impact of local isotopic fractionation in the measurements. In that
 600 sense, although the measurements made by the SAM/TLS are more precise, they are more
 601 constrained in terms of location, season, and local time sampling, where the contribu-
 602 tion from climatological fractionation is unknown.

603 Using the approach of Jakosky (2019), we estimate the amount of C lost to space
 604 through time considering the implications of our measurements of the $^{13}\text{C}/^{12}\text{C}$ ratio. In
 605 particular, if considering that the difference between the SAM/TLS and ACS measure-

606 ments arises from fractionation between the lower and upper atmospheres of Mars, we
 607 estimate that at least 40% of the C reservoir on Mars would have been lost to space through-
 608 out history. On the other hand, if the C isotopic composition of the present-day atmo-
 609 sphere follows the values derived in this study, we estimate that at least 20% of C would
 610 have been lost. These estimates represent a lower limit on the amount of C lost to space
 611 since other processes such as outgassing or carbonate formation would produce a rela-
 612 tive depletion of the heavy isotopes in the atmosphere.

613 Finally, we compare the $^{18}\text{O}/^{16}\text{O}$ isotopic ratio in H_2O ($\delta^{18}\text{O}(\text{H}_2\text{O}) = 140 \pm 80$
 614 ‰) and CO_2 ($\delta^{18}\text{O}(\text{CO}_2) = -29 \pm 38$ ‰), which indicates that the former is more en-
 615 riched in the heavy isotope. The isotopic ratios in these two species can be different if
 616 oxygen is exchanging between them and the isotopes are preferentially transferred to one
 617 species over the other. We propose that the enrichment in the heavy isotopes of H_2O
 618 over CO_2 might be explained by a transfer of light O from H_2O to CO_2 by photochem-
 619 ical reactions involving the photolysis of these two species, and the posterior recombini-
 620 nation of the photolysis products into CO_2 .

621 **Appendix A Validation of the retrieval scheme using synthetic spec-** 622 **tra**

623 The retrieval scheme presented in this study utilises a simple description of the ra-
 624 diative transfer calculations, which assume that the gaseous absorption occurs over a ho-
 625 mogeneous path with constant pressure and temperature. In order to analyse the valid-
 626 ity and accuracy of this method, a series of retrieval tests are performed using synthetic
 627 spectra. The synthetic spectra are generated using the full radiative transfer calculations
 628 from the NEMESIS algorithm (Irwin et al., 2008), which split the atmosphere into sev-
 629 eral layers with different pressure and temperature, and therefore provide a more real-
 630 istic representation of the atmosphere.

631 The reference profiles used to generate the synthetic spectra are taken from the Mars
 632 Climate Database (MCD) (Forget et al., 1999), using the same observational paramet-
 633 ers (i.e., latitude, longitude, L_S and local time) as the ACS MIR observations made dur-
 634 ing MY34. Since the MCD does not provide atmospheric profiles for the isotopic ratios,
 635 these are generated using equation 5. In particular, we assume random values of the dif-
 636 ferent isotopic ratios below the homopause ($0.7 \leq R_h \leq 1.3$ VPDB or VSMOW), the
 637 altitude of the homopause ($90 \leq z_h \leq 110$ km) and the temperature ($100 \leq T \leq 140$
 638 K) for each observation. Using these reference atmospheric profiles for the different species,
 639 we generate transmission spectra from 70 to 130 km and add random noise following a
 640 Gaussian distribution corresponding to a signal-to-noise ratio (SNR) of 5000, which aim
 641 to replicate the ACS MIR measurements.

642 Once the transmission spectra are generated, these are retrieved using the scheme
 643 presented in this study, which assumes a constant pressure and temperature along the
 644 path. The results of these retrievals are summarised in Figure A1, which shows the dif-
 645 ference between the retrieved isotopic ratios and the ones that were used to generate the
 646 synthetic spectra at each altitude for the different observations. In the case that no sys-
 647 tematic biases exist, one may expect the average value of these differences to be centred
 648 at zero, with some standard deviation representative of the uncertainty of the retrieval.
 649 While this is the case for the retrieval of the $^{13}\text{C}/^{12}\text{C}$ isotopic ratio, Figure A1 suggests
 650 a systematic bias in the retrieval of the O isotopic ratios that varies with altitude. In
 651 particular, while the convergence between the retrieved and real ratios is good near 70
 652 km, the retrieved isotopic ratios are systematically ~ 0.05 VSMOW higher than the ones
 653 that were used to generate the synthetic spectra at 100 km. The source of this overes-
 654 timation of the O isotopic ratios is most likely related to the simplified radiative trans-
 655 fer calculations used in this study. For example, while it is assumed that the tempera-
 656 ture field is constant along the path, the averaging kernels shown in Figure 3 indicate

657 that the spectra is sensitive to the layers a few kilometres above the tangent point, which
 658 can produce a bias in the retrieved isotopic ratios if there are strong temperature vari-
 659 ations along the line of sight. This systematic bias is also expected to occur in the ACS
 660 MIR retrievals and might cause an unreal increase of the retrieved isotopic ratios with
 661 altitude, which must be taken into account when analysing the altitude variations of the
 662 isotopic ratios.

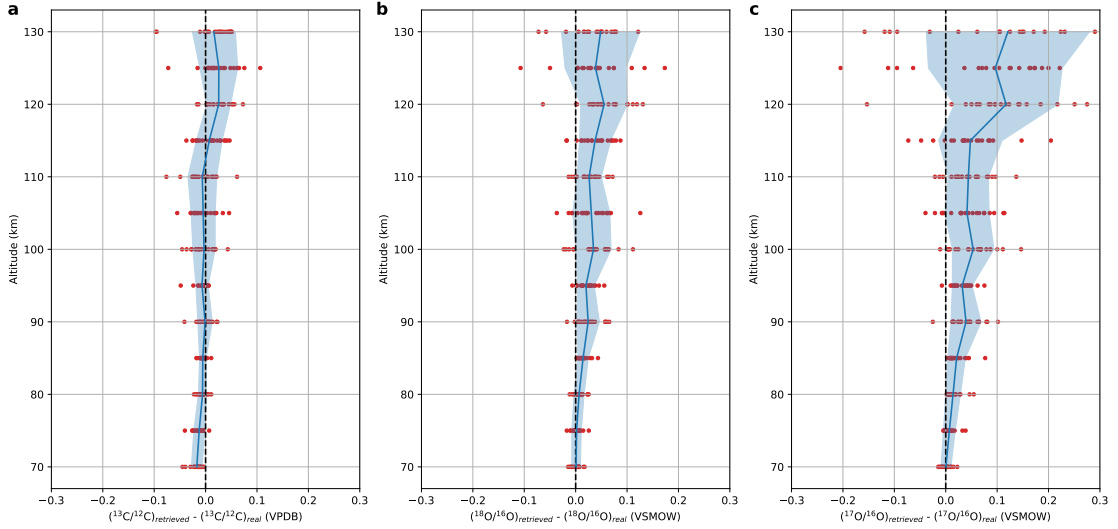


Figure A1. Validation of the retrieval scheme using synthetic spectra. The different panels show the difference between the retrieved $^{13}\text{C}/^{12}\text{C}$ (a), $^{18}\text{O}/^{16}\text{O}$ (b) and $^{17}\text{O}/^{16}\text{O}$ (c) isotopic ratios and the ones that were used to generate the synthetic spectra at each altitude level. The red points represent the values derived from each observation, while the blue lines and shared regions represent the mean and standard deviation of these points at each level. While the mean value of the differences in the $^{13}\text{C}/^{12}\text{C}$ ratio is close to zero at all altitudes, this quantity reveals a systematic bias in the retrievals of the $^{18}\text{O}/^{16}\text{O}$ and $^{17}\text{O}/^{16}\text{O}$ ratios, which tend to overestimate the isotopic ratio.

Acknowledgments

663 We thank the reviewers, Timothy A. Livengood and Shohei Aoki, for their useful crit-
 664 icism and suggestions for improvement. The ExoMars mission is a joint mission of the
 665 European Space Agency (ESA) and Roscosmos. The ACS experiment is led by the Space
 666 Research Institute (IKI) in Moscow, assisted by LATMOS in France. This work was funded
 667 by Roscosmos, the National Centre for Space Studies of France (CNES), the Ministry
 668 of Science and Education of Russia, the Natural Sciences and Engineering Research Coun-
 669 cil of Canada (NSERC) (PDF 178 - 516895 - 2018), and the UK Space Agency (ST/T002069/1,
 670 ST/R001502/1 and ST/P001572/1).
 671

Data availability

672 The datasets generated by the ExoMars Trace Gas Orbiter instruments analysed
 673 in this study are available in the ESA Planetary Science Archive (PSA) repository, [https://
 674 archives.esac.esa.int/psa/#!Table%20View/ACS=instrument](https://archives.esac.esa.int/psa/#!Table%20View/ACS=instrument), following a six months
 675 prior access period, following the ESA Rules on Information, Data and Intellectual Prop-
 676 erty. The spectral fitting and retrievals were performed using the NEMESIS radiative
 677

678 transfer and retrieval algorithm (Irwin et al., 2008) and can be downloaded from Irwin
 679 (2020). The data products generated in this study (retrieved atmospheric parameters)
 680 are available on Alday (2021).

681 References

- 682 Alday, J. (2021). *Isotopic composition of H₂O and CO₂ on Mars from ACS MIR so-*
 683 *lar occultations*. Zenodo. (Version v01) doi: 10.5281/zenodo.5100449
- 684 Alday, J., Trokhimovskiy, A., Irwin, P. G. J., Wilson, C. F., Montmessin, F.,
 685 Lefvre, F., ... Shakun, A. (2021). Isotopic fractionation of water and its
 686 photolytic products in the atmosphere of Mars. *Nature Astronomy*. doi:
 687 10.1038/s41550-021-01389-x
- 688 Alday, J., Wilson, C. F., Irwin, P. G. J., Olsen, K. S., Baggio, L., Montmessin, F.,
 689 ... Shakun, A. (2019). Oxygen isotopic ratios in Martian water vapour ob-
 690 served by ACS MIR on board the ExoMars Trace Gas Orbiter. *Astronomy &*
 691 *Astrophysics*, 630, A91. doi: 10.1051/0004-6361/201936234
- 692 Baker, V. R. (2001). Water and the martian landscape. *Nature*, 412(6843), 228–236.
 693 doi: 10.1038/35084172
- 694 Carr, M. H., & Clow, G. D. (1981). Martian channels and valleys: Their character-
 695 istics, distribution, and age. *Icarus*, 48(1), 91–117. doi: 10.1016/0019-1035(81)
 696 90156-1
- 697 Cui, J., Wu, X. S., Gu, H., Jiang, F. Y., & Wei, Y. (2019, January). Photochemical
 698 escape of atomic C and N on Mars: clues from a multi-instrument MAVEN
 699 dataset. *Astronomy & Astrophysics*, 621, A23. doi: 10.1051/0004-6361/
 700 201833749
- 701 Eiler, J. M., Kitchen, N., & Rahn, T. A. (2000). Experimental constraints on
 702 the stable-isotope systematics of CO₂ ice/vapor systems and relevance to
 703 the study of Mars. *Geochimica et Cosmochimica Acta*, 64(4), 733–746. doi:
 704 10.1016/S0016-7037(99)00327-0
- 705 Encrenaz, T., Bezdard, B., Owen, T., Lebonnois, S., Lefevre, F., Greathouse, T.,
 706 ... Wong, A. (2005). Infrared imaging spectroscopy of Mars: H₂O map-
 707 ping and determination of CO₂ isotopic ratios. *Icarus*, 179(1), 43–54. doi:
 708 10.1016/j.icarus.2005.06.022
- 709 Fedorova, A. A., Montmessin, F., Korablev, O., Luginin, M., Trokhimovskiy, A.,
 710 Belyaev, D. A., ... Wilson, C. F. (2020). Stormy water on Mars: The distri-
 711 bution and saturation of atmospheric water during the dusty season. *Science*,
 712 367(6475), 297–300. doi: 10.1126/science.aay9522
- 713 Forget, F., Hourdin, F., Fournier, R., Hourdin, C., Talagrand, O., Collins, M., ...
 714 Huot, J.-P. (1999). Improved general circulation models of the Martian at-
 715 mosphere from the surface to above 80 km. *Journal of Geophysical Research:*
 716 *Planets*, 104(E10), 24155–24175. doi: 10.1029/1999JE001025
- 717 Fox, J. L., & Bakalian, F. M. (2001, December). Photochemical escape of atomic
 718 carbon from Mars. *Journal of Geophysical Research: Space Physics*, 106(A12),
 719 28785–28795. doi: 10.1029/2001JA000108
- 720 Fox, J. L., & Ha, A. (1999). Velocity distributions of C atoms in CO⁺ dissociative
 721 recombination: Implications for photochemical escape of C from Mars. *Journal*
 722 *of Geophysical Research: Space Physics*, 104(A11), 24729–24737. doi: 10.1029/
 723 1999JA900330
- 724 Gamache, R. R., Roller, C., Lopes, E., Gordon, I. E., Rothman, L. S., Polyansky,
 725 O. L., ... Kochanov, R. V. (2017). Total internal partition sums for 166 iso-
 726 topologues of 51 molecules important in planetary atmospheres: Application to
 727 HITRAN2016 and beyond. *Journal of Quantitative Spectroscopy and Radiative*
 728 *Transfer*, 203, 70–87. doi: 10.1016/j.jqsrt.2017.03.045
- 729 Gordon, I., Rothman, L., Hill, C., Kochanov, R., Tan, Y., Bernath, P., ... Zak,
 730 E. (2017). The HITRAN2016 molecular spectroscopic database. *Jour-*

- 731 *nal of Quantitative Spectroscopy and Radiative Transfer*, 203, 3–69. doi:
732 10.1016/j.jqsrt.2017.06.038
- 733 Grller, H., Lichtenegger, H., Lammer, H., & Shematovich, V. (2014, August). Hot
734 oxygen and carbon escape from the martian atmosphere. *Planetary and Space*
735 *Science*, 98, 93–105. doi: 10.1016/j.pss.2014.01.007
- 736 Hase, F., Wallace, L., McLeod, S. D., Harrison, J. J., & Bernath, P. F. (2010). The
737 ACE-FTS atlas of the infrared solar spectrum. *Journal of Quantitative Spec-*
738 *troscopy and Radiative Transfer*, 111(4), 521–528. doi: 10.1016/j.jqsrt.2009.10
739 .020
- 740 Hu, R., Kass, D. M., Ehlmann, B. L., & Yung, Y. L. (2015). Tracing the fate of
741 carbon and the atmospheric evolution of Mars. *Nature Communications*, 6(1),
742 10003. doi: 10.1038/ncomms10003
- 743 Irwin, P. (2020). *NEMESIS/Radtrancode Software*. Zenodo. doi: 10.5281/zenodo
744 .4303976
- 745 Irwin, P., Teanby, N., de Kok, R., Fletcher, L., Howett, C., Tsang, C., ... Parrish,
746 P. (2008). The NEMESIS planetary atmosphere radiative transfer and re-
747 trieval tool. *Journal of Quantitative Spectroscopy and Radiative Transfer*,
748 109(6), 1136–1150. doi: 10.1016/j.jqsrt.2007.11.006
- 749 Jakosky, B. M. (1991). Mars volatile evolution: Evidence from stable isotopes.
750 *Icarus*, 94(1), 14–31. doi: 10.1016/0019-1035(91)90138-J
- 751 Jakosky, B. M. (1997). Evolution of the Martian atmosphere. *Advances in Space Re-*
752 *search*, 19(8), 1289. doi: 10.1016/S0273-1177(97)83130-4
- 753 Jakosky, B. M. (2019). The CO₂ inventory on Mars. *Planetary and Space Science*,
754 175, 52–59. doi: 10.1016/j.pss.2019.06.002
- 755 Jakosky, B. M., Pepin, R. O., Johnson, R. E., & Fox, J. (1994). Mars Atmospheric
756 Loss and Isotopic Fractionation by Solar-Wind-Induced Sputtering and Photo-
757 chemical Escape. *Icarus*, 111(2), 271–288. doi: 10.1006/icar.1994.1145
- 758 Jakosky, B. M., Slipski, M., Benna, M., Mahaffy, P., Elrod, M., Yelle, R., ... Al-
759 saeed, N. (2017, March). Mars atmospheric history derived from upper-
760 atmosphere measurements of ³⁸Ar/³⁶Ar. *Science*, 355(6332), 1408–1410. doi:
761 10.1126/science.aai7721
- 762 Korablev, O., Montmessin, F., Trokhimovskiy, A., Fedorova, A. A., Shakun, A. V.,
763 Grigoriev, A. V., ... Zorzano, M. P. (2018). The Atmospheric Chemistry Suite
764 (ACS) of Three Spectrometers for the ExoMars 2016 Trace Gas Orbiter. *Space*
765 *Science Reviews*, 214(1), 7. doi: 10.1007/s11214-017-0437-6
- 766 Krasnopolsky, V. A., Maillard, J. P., Owen, T. C., Toth, R. A., & Smith, M. D.
767 (2007). Oxygen and carbon isotope ratios in the martian atmosphere. *Icarus*,
768 192(2), 396–403. doi: 10.1016/j.icarus.2007.08.013
- 769 Krasnopolsky, V. A., Mumma, M., Bjoraker, G., & Jennings, D. (1996). Oxy-
770 gen and Carbon Isotope Ratios in Martian Carbon Dioxide: Measurements
771 and Implications for Atmospheric Evolution. *Icarus*, 124(2), 553–568. doi:
772 10.1006/icar.1996.0230
- 773 Livengood, T. A., Kostiuik, T., Hewagama, T., Smith, R. L., Fast, K. E., An-
774 nen, J. N., & Delgado, J. D. (2020). Evidence for diurnally varying en-
775 richment of heavy oxygen in Mars atmosphere. *Icarus*, 335, 113387. doi:
776 10.1016/j.icarus.2019.113387
- 777 Mahaffy, P. R., Webster, C. R., Atreya, S. K., Franz, H., Wong, M., Conrad, P. G.,
778 ... Moores, J. E. (2013). Abundance and Isotopic Composition of Gases in the
779 Martian Atmosphere from the Curiosity Rover. *Science*, 341(6143), 263–266.
780 doi: 10.1126/science.1237966
- 781 Mahieux, A., Vandaele, A. C., Neefs, E., Robert, S., Wilquet, V., Drummond, R., ...
782 Bertaux, J. L. (2010). Densities and temperatures in the Venus mesosphere
783 and lower thermosphere retrieved from SOIR on board Venus Express: Re-
784 trieval technique. *Journal of Geophysical Research*, 115(E12), E12014. doi:
785 10.1029/2010JE003589

- 786 Martn-Torres, F. J., Zorzano, M.-P., Valentn-Serrano, P., Harri, A.-M., Genzer, M.,
 787 Kemppinen, O., ... Vaniman, D. (2015). Transient liquid water and wa-
 788 ter activity at Gale crater on Mars. *Nature Geoscience*, 8(5), 357–361. doi:
 789 10.1038/ngeo2412
- 790 McElroy, M. B. (1972, January). Mars: An Evolving Atmosphere. *Science*,
 791 175(4020), 443–445. doi: 10.1126/science.175.4020.443
- 792 McElroy, M. B., & Donahue, T. M. (1972). Stability of the Martian Atmosphere.
 793 *Science*, 177(4053), 986–988. doi: 10.1126/science.177.4053.986
- 794 Miller, C. E., & Yung, Y. L. (2000). Photo-induced isotopic fractionation. *Journal*
 795 *of Geophysical Research: Atmospheres*, 105(D23), 29039–29051. doi: 10.1029/
 796 2000JD900388
- 797 Nier, A. O., & McElroy, M. B. (1977). Composition and structure of Mars' Up-
 798 per atmosphere: Results from the neutral mass spectrometers on Viking
 799 1 and 2. *Journal of Geophysical Research*, 82(28), 4341–4349. doi:
 800 10.1029/JS082i028p04341
- 801 Niles, P. B., Boynton, W. V., Hoffman, J. H., Ming, D. W., & Hamara, D. (2010).
 802 Stable Isotope Measurements of Martian Atmospheric CO₂ at the Phoenix
 803 Landing Site. *Science*, 329(5997), 1334–1337. doi: 10.1126/science.1192863
- 804 Niles, P. B., Mahaffy, P. R., Atreya, S., Pavlov, A. A., Trainer, M., Webster, C. R.,
 805 & Wong, M. (2014). Reconciling the Differences Between the Measurements of
 806 CO₂ Isotopes by the Phoenix and MSL Landers. In (p. 2573).
- 807 Olsen, K. S., Lefvre, F., Montmessin, F., Fedorova, A. A., Trokhimovskiy, A., Bag-
 808 gio, L., ... Shakun, A. (2021). The vertical structure of CO in the Martian
 809 atmosphere from the ExoMars Trace Gas Orbiter. *Nature Geoscience*, 14,
 810 67–71. doi: 10.1038/s41561-020-00678-w
- 811 Olsen, K. S., Toon, G. C., Boone, C. D., & Strong, K. (2016). New temper-
 812 ature and pressure retrieval algorithm for high-resolution infrared solar
 813 occultation spectroscopy: analysis and validation against ACE-FTS and
 814 COSMIC. *Atmospheric Measurement Techniques*, 9(3), 1063–1082. doi:
 815 10.5194/amt-9-1063-2016
- 816 Owen, T. (1982). The composition of the martian atmosphere. *Advances in Space*
 817 *Research*, 2(2), 75–80. doi: 10.1016/0273-1177(82)90107-7
- 818 Owen, T., Biemann, K., Rushneck, D. R., Biller, J. E., Howarth, D. W., &
 819 Lafleur, A. L. (1977). The composition of the atmosphere at the sur-
 820 face of Mars. *Journal of Geophysical Research*, 82(28), 4635–4639. doi:
 821 10.1029/JS082i028p04635
- 822 Qumerais, E., Bertaux, J.-L., Korablev, O., Dimarellis, E., Cot, C., Sandel,
 823 B. R., & Fussen, D. (2006). Stellar occultations observed by SPICAM on
 824 Mars Express. *Journal of Geophysical Research*, 111(E9), E09S04. doi:
 825 10.1029/2005JE002604
- 826 Rahn, T., & Eiler, J. (2001). Experimental constraints on the fractionation of
 827 ¹³C/¹²C and ¹⁸O/¹⁶O ratios due to adsorption of CO₂ on mineral substrates
 828 at conditions relevant to the surface of Mars. *Geochimica et Cosmochimica*
 829 *Acta*, 65(5), 839–846. doi: 10.1016/S0016-7037(00)00592-5
- 830 Ramirez, R. M., Kopparapu, R., Zuger, M. E., Robinson, T. D., Freedman, R.,
 831 & Kasting, J. F. (2014). Warming early Mars with CO₂ and H₂. *Nature*
 832 *Geoscience*, 7(1), 59–63. doi: 10.1038/ngeo2000
- 833 Rodgers, C. D. (2000). *Inverse Methods for Atmospheric Sounding: Theory and*
 834 *Practice* (Vol. 2). World Scientific. doi: 10.1142/3171
- 835 Schmidt, J. A., Johnson, M. S., & Schinke, R. (2013). Carbon dioxide photolysis
 836 from 150 to 210 nm: Singlet and triplet channel dynamics, UV-spectrum, and
 837 isotope effects. *Proceedings of the National Academy of Sciences*, 110(44),
 838 17691–17696. doi: 10.1073/pnas.1213083110
- 839 Schrey, U., Rothermel, H., Kaufl, H. U., & Drapatz, S. (1986). Determination of
 840 the C-12/C-13 and O-16/O-18 ratio in the Martian atmosphere by 10 micron

- 841 heterodyne spectroscopy. *Astronomy and Astrophysics*, 155, 200–204.
- 842 Slipski, M., Jakosky, B., Benna, M., Elrod, M., Mahaffy, P., Kass, D., . . . Yelle, R.
843 (2018). Variability of Martian Turbopause Altitudes. *Journal of Geophysical*
844 *Research: Planets*, 123(11), 2939–2957. doi: 10.1029/2018JE005704
- 845 Urey, H. C. (1947). The thermodynamic properties of isotopic substances. *Journal of*
846 *the Chemical Society (Resumed)*, 562. doi: 10.1039/jr9470000562
- 847 Webster, C. R., Mahaffy, P. R., Flesch, G. J., Niles, P. B., Jones, J. H., Leshin,
848 L. A., . . . the MSL Science Team (2013). Isotope Ratios of H, C, and O in
849 CO₂ and H₂O of the Martian Atmosphere. *Science*, 341(6143), 260–263. doi:
850 10.1126/science.1237961
- 851 Wordsworth, R., Forget, F., Millour, E., Head, J., Madeleine, J.-B., & Charnay,
852 B. (2013). Global modelling of the early martian climate under a denser
853 CO₂ atmosphere: Water cycle and ice evolution. *Icarus*, 222(1), 1–19. doi:
854 10.1016/j.icarus.2012.09.036
- 855 Wright, I., Carr, R., & Pillinger, C. (1986). Carbon abundance and isotopic stud-
856 ies of Shergotty and other shergottite meteorites. *Geochimica et Cosmochimica*
857 *Acta*, 50(6), 983–991. doi: 10.1016/0016-7037(86)90379-0
- 858 Young, E. D., Galy, A., & Nagahara, H. (2002). Kinetic and equilibrium mass-
859 dependent isotope fractionation laws in nature and their geochemical and cos-
860 mochemical significance. *Geochimica et Cosmochimica Acta*, 66(6), 1095–1104.
861 doi: 10.1016/S0016-7037(01)00832-8